Universität Hamburg
DER FORSCHUNG | DER LEHRE | DER BILDUNG

bachelor thesis

Investigations and Considerations of Oxygen Diffusion Profiles in Superconducting Mid-T RF Cavities Utilizing EXAFS Spectroscopy

Niels Eckert

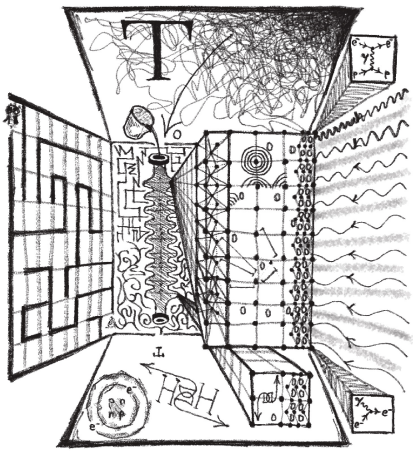

Submitted on 20. October 2025

Physics B.Sc.
Matriculation number: 7615659
Mail address: niels.eckert@proton.me

Supervisors:
1st Prof. Dr. Wolfgang Hillert
2nd Dr. Marc Wenskat

Für meine Oma

&

jene, die mit meinem Opa für sie da sind.

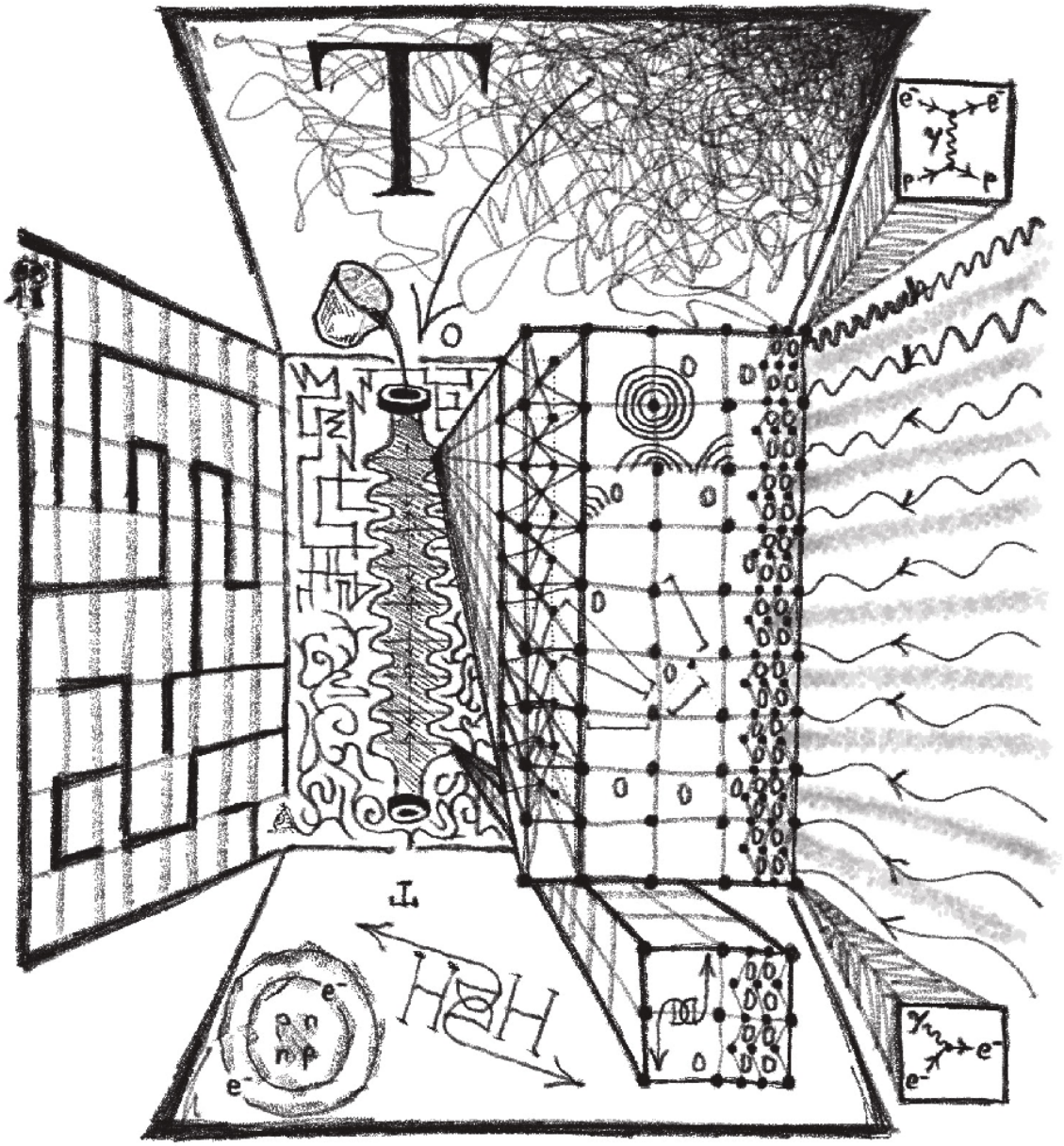
T
e⁻
e⁻
γ
p
p
e⁻
p n
n p
e⁻
γ
e⁻
e⁻

Zusammenfassung

Die Untersuchung von Sauerstofftiefenprofilen in mid-T behandelten SRF Kavitäten ist zentral, um physikalische Zusammenhänge zwischen dem mikroskopischen Kavitätengitter und der entsprechenden Leistungsfähigkeit im Betrieb entschlüsseln zu können – eine Fragestellung, die Beschleunigungsphysiker/innen seit Jahren beschäftigt. Diese Arbeit bietet die Analyse dieser Profile dreier unterschiedlich behandelter Proben: Zwei des mid-T Typs und die Dritte nach bewährtem EuXFEL Rezept. Die Messmethode greift auf die EXAFS-Spektroskopie zurück und wurde am DELTA Speicherring in Dortmund durchgeführt. Das Ergebnis ist stark verrauscht und erlaubt kaum quantitative Rückschlüsse. Qualitativ konnte keine Abweichung der Profile von gängigen Modellen nachgewiesen werden, wie auch die Messungen nicht im Widerspruch zu vorigen Untersuchungen stehen. Nichtsdestotrotz wird das Vorgehen im Experiment bis ins Detail dokumentiert, Interpretationen, soweit möglich, vorgenommen und theoretische Überlegungen, bezüglich der Fehlerabschätzung und potentieller EXAFS-Simulationen, für künftige Forschungen angestellt.
Ein erneuter Anlauf an der PETRA III Anlage wird vorgeschlagen.

Abstract

A screening of oxygen profiles in mid-T treated SRF cavities is crucial, in order to infer physical correlations between the microscopic cavity lattice and cavity performance – a problem concerning acceleration physicists for years. This thesis provides an analysis of oxygen diffusion profiles for three differently treated samples: Two mid-T baked and the third with the standard EuXFEL recipe. The measurement method utilizes EXAFS spectroscopy and was carried out at the DELTA facility in Dortmund. The result suffers heavily under noise, making the quantity of the result barely useable. Qualitatively, no deviations of current models regarding the profiles, could be proven, and no results of previous studies were contradicted. The experimental analysis is described in precision, interpretations of the possible are undertaken and theoretical considerations regarding error estimation and possible EXAFS simulations for future attempts are provided. A repitition at the PETRA III facility is indicated.

Contents

1 Introduction **1**

2 Self Referenciality **2**

3 Foundations of SRF Cavities and Crystallographic Dynamics **3**

3.1 Importance of SRF Cavities for Accelerator Physics 3

3.2 Groundwork of Superconductors 5

3.3 Mid-T Bake of SRF Cavities 6

3.4 Principles of Atomic Diffusion 7

3.5 Theory of EXAFS 8

4 Characterization of Sample Treatments **12**

5 Inductive EXAFS Examination of Niobium Samples **13**

5.1 Setup of the Beamline Experiment 14

5.2 Acquisition of Measurement Spectra 14

5.3 Extracting the Fine Structure 16

5.4 Results 18

6 Error Analysis in XAFS **24**

7 Considerations for EXAFS Simulations **25**

8 Discussion of Results and Method **26**

8.1 Error Discussion 26

8.2 Methodological Comparison 29

8.3 Outlook 29

9 Conclusion **31**

References **34**

A Raw Measurements **35**

B Peak Migration **36**

C Error Plots **39**

D Basic Terms of Self-Referencing Systems **40**

Acknowledgements **42**

1 Introduction

With the historical implementation of superconductivity in the field of radio frequency (RF) cavities in the $1990\mathrm{s}$, major progress was made in terms of the operation and development of modern particle accelerators, utilized especially in particle physics, material science, biology and medicine. This progress can be expressed by the ~ 6 orders of magnitude improved quality factor of SRF cavities, compared to normally conducting ones.[Ale] This is causing an enormous reduction in needed RF energy accordingly and outweighing additional cooling costs below critical temperature. Accelerators like the European XFEL in Hamburg and the LCLS-II at SLAC in Stanford are already based on this SRF technology and even the LHC at CERN near Geneva uses partially superconducting cavities, in order to benefit from their advantages. Damages and impurities of the surface during the cavity fabrication process led to the standard procedure of performing chemical and heat treatments of SRF cavities before usage in acceleration operation, in order to polish and purify their surfaces. The unexpected observation of quality factor improvements due to intentional impurities of certain elements on the other hand, initiated the effort of analyzing those improvements extent and understanding it's theoretical background, up until today. A promising approach in recent years hereby, are heat treatments in the medium temperature range between roughly $200\,^{\circ}\mathrm{C}$ and $400\,^{\circ}\mathrm{C}$, thus called mid-T baking, where oxygen atoms on the surface due to the natural oxidation process of the cavity metal exposed to air, are expected to diffuse further into the surface.[Pos+19] The conventional model of Fickian diffusion suggests in this case an oxygen diffusion profile which is based on the cavity metal beeing a perfect crystal lattice. Crystal defects, especially grains, suggest this profile applies over long distances, but that inhomogeneous diffusion in the near-surface range cannot average out and thus causes deviations. This thesis addresses this question by analyzing mid-T treated samples in terms of their oxygen concentration profile in the near-surface range and furthermore carries out a comparison with the treatment recipe performed for the (already in operation) EuXFEL cavities. First, in section 3 major concepts in the context of this analysis are introduced, in section 4 the samples are reviewed, followed by the description and evaluation of an experiment at the DELTA accelerator at TU Dortmund in section 5, with which the samples have been analyzed. The underlying method of investigation is utilizing EXAFS spectroscopy in fluoresence mode, which is determining the samples crystal structure through absorption measurements of X-rays. This approach was already pursued last year by Luth [Lut24] and turned out to suffer heavily on measurement noise. The lessons we have learned in terms of the experimental execution, motivated a second attempt, which is presented here. Let it be said in advance, that data quality didn't improve significantly, thus a detailed analysis of what is possible and general considerations regarding error analysis (section 6) are undertaken. Moreover, the aim of simulating an EXAFS measurement, in order to judge whether the EXAFS measurements agree with presumptions of the sample lattices, is pursued (see section 7). For this, two software programs are in consideration. In section 8, errors and method are discussed, alternative techniques of analysis pointed out, and an outlook for future research is provided. Additionally, section 2 proposes an unconventional analysis for a thesis, focusing on self referencing structures that arise in the context of this study.

2 Self Referenciality

This section carries out the proposed program of the last paragraph in appendix D for the context of the present thesis, using the terms introduced in it's previous paragraphs. References to the relevant sections in this thesis are provided.

seref · *launism* · *calcism* · *serlau pleasure* · *serlau doubt* · *flarameter*

Seref contexts can be recognized in terms of the description of XAFS spectroscopy as a whole, it's error analysis, the beamline experiment at the DELTA facility, the mysterious effect of impurities on cavity performance and benefits of the SRF technology overall.

First of all, XAFS depends on scattering processes, the implications of which were of great debate during the last decades and is up until today (see sec. 3.5, [Lyt00]). Because the behaviour of the photo electron depends on scattering, whose stimulation depends on the photo electron again, XAFS shows seref properties. The launistic attempts of describing XAFS in a calculistic manner in the community can be taken as opportunity for the serlau pleasure induced proposition, that upcoming thoughts will result into a deeper description of XAFS, eliminating the need for comparing XAFS spectra with literature in order to gain information about the single measurement.

Connected to that is the current widespread handling of not calculating uncertainties for XAFS spectra in the community (see sec. 6, [BH09], [MSN81]). Error estimation serves the purpose of comparing different measurements with one another, to consult on a rating in the seref context of society (and rather not to state a *true error*, because it has no clear definition). Thus the proposition of no need for error estimation, can be doubted serlauily by stating that the seref scientific discussion relies on transparent uncertainties.

Moreover, regarding the specific EXAFS experiment in this thesis (see sec. 5), the situation unfolds that samples got analyzed via radiation of an acceleration facility. The outcome of which is dedicated to improve those acceleration facilities themselves. This obvious seref relationship refers to the reliability of particle dynamics and production of synchrotron radiation. Thus, the performed EXAFS analysis in this thesis is potentially vulnerable to serlau doubts, stating that the SRF-expertise through this kind of analysis is contradicting itself and the acceleration process is indeed incorrectly described. But this could only apply in the very bold case that main groundwork on particle acceleration and synchrotron radiation was false all along.

Furthermore, the empirical observation that cavity impurities cause a lowering of the surface resistance and thus improvements in the Q curve (see sec. 3.3), raises questions about the BCS theory and the interaction of particles in electrical current with the cavity lattice. The whole BCS theory in the postulate of Cooper pairs and how they emerge (see sec. 3.2), utilizes principles and methods of quantum physics which are deeply seref.[1]

[1] As expressed in the materialistic illustration by Werner Heisenberg in 1965, that the uncertainty principle can be understood as lack of knowledge of both position and momentum of an electron, because each position measurement via a photon influences it's momentum and vice versa.

This would allow the serlau induced proposition, that oxygen interstitials intermediate the emergence of other Cooper pairs (other than electrons) in order to cause an effect not present in pure cavities.

And finally, the main benefits of SRF cavities, which lie in the lower energy consumption and thus, not least, in the saving of research costs, connects to the seref system of society. Therefore serlau induced propositions about the behaviour of society, can lead to inspiration regarding strategic research in order to ongoingly satisfy curiosity. Such seref propositions may say something about the political community deciding about research funding or the economic system as a whole. Time as the flarameter will continuously raise new situations.

3 Foundations of SRF Cavities and Crystallographic Dynamics

To fully understand the following analysis of SRF cavity lattices, it is necessary to be clear about some underlying knowledge and concepts in accelerator physics, low temperature physics, thermodynamics and atomic spectroscopy. Thus I summarize the significance of cavity structures for the field of accelerator physics, aspecially in the realization of the superconducting accelerator technology. So called mid-T heat treatments of SRF cavities are beeing explained, followed by an introduction into the diffusion principles which are crucial for describing the heating processes appropriately. Lastly, the atomic physics theory of EXAFS is discussed, in order to disclose the analyzation method for the oxygen concentrations in the niobium lattice.

3.1 Importance of SRF Cavities for Accelerator Physics

The history of acceleration facilities has gone through many steps throughout the 20th century, steadily increasing their performance and applicability. Currently, the technological gold standard in accelerating relativistic particles are cavity resonators, in which an alternating electromagnetic field is induced at radio frequency[2] and the particles are accelerated by the Coulomb force due to that field mode. The conceivable cavity shapes are diverse and fulfill various optimization requirements (for the EM fields, those modes decisively depend on the resonator shape), like field magnitudes on the beam axis or transverse beam focussing. Here a currently important standard is given by the *TESLA* shape introduced in 2000[3].[Aun+00] The TESLA standard is designed for superconducting operation, meaning those cavities consist of niobium and are cooled in order to enter the superconducting phase, which led to the need of a cumbersome cryogenic infrastructure around the cavities while accelerating. The benefit on the other hand is a massive improvement of the (oscillation related) quality factor of the field modes; while copper cavities show Q factors of about 10^4, superconducting niobium cavities reach values in the order of 10^{10}.[Ale] It is calculated in general by

$$Q = \frac{\omega U}{P_{\text{diss}}} \tag{1}$$

[2] Radio frequency ranges per definition between 20 kHz and 300 GHz, while in accelerators frequencies in the range of GHz are commonly used.

[3] Cavities in the TESLA shape are already installed e.g. in the EuXFEL and furthermore intended to be installed in the yet to be planned and build international linear collider (ILC).

with the cavity modes eigenfrequency ω, the stored energy in the cavity U and the dissipated power into the cavity wall P_{diss}. These quantities are useful for measuring Q, but it is of interest as well to express it in terms of the surface resistance R_{s} of the cavity, which is possible via the expression

$$Q = \frac{G}{R_{\text{s}}} \tag{2}$$

because P_{diss} is proportional to R_{s}[4]. For a given field mode G represents a purely geometric factor, independent of material properties.

When analyzing the performance of an SRF cavity, the Q value gets important. In test facilities like the AMTF at DESY, such performance tests are run systematically by successively increasing the EM field inside the cavity. The result is characterized by the *quality curve*, where the Q factor is plotted against the acceleration gradient E_{acc} (average electric field, which the accelerating particle is exposed to, during it's flight through the cavity). In (BCS) theory, the Q curve would be assumed constant until the cavity quenches.[Web08] However, we see multiple phenomena in experiments that prove differently. First there is an increase in Q for small values of E_{acc} (low field), a slight drop for medium values (medium field) and a very steep drop for high values (high field) (see fig. 1a). In some cases of heat treatments (see sec. 3.3) we instead see an increase in the medium field (named *anti-Q-slope*, see fig. 1b). Aspecially the high-field Q slope (often referred to as HFQS or just Q-*drop*) is of great interest and limits the possibilities of cavities, it is historically usually called the 'European headache'.[Bau+06]

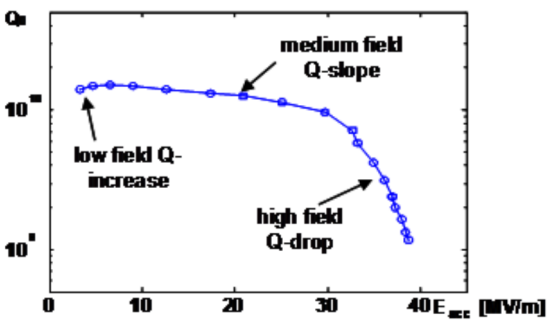

(a) Schematic Q curve of cavities in performance tests. All three regimes (low-, medium- and high-field) are part of current research.[Bau+06]

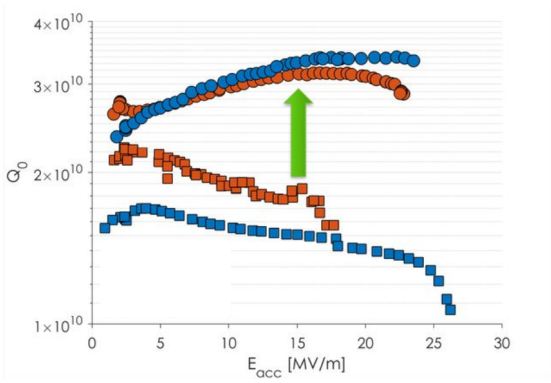

(b) Comparison of two cavity Q curves both before (MF Q-slope, squares) and after (anti-Q-slope, circles) a specific treatment demonstrates improvements in the Q factor. Data taken at SLAC.

Figure 1

The explanation is subject of current research and, not least, this thesis. But assumed are loss mechanisms which depend on the accelerating field and make it at least comprehensible, to see those phenomena.[Web08]

[4] It is assumed R_{s} is constant over the cavity surface.

3.2 Groundwork of Superconductors

Superconductors as they are utilized for particle acceleration as SRF cavities, originate in the phenomenon of a completely vanishing electrical resistance for some conductors under specific circumstances. Those circumstances are a temperature below some critical value T_c, a possibly existing external magnetic field underneath a threshold H_{c1} (both material-dependent) and an applied DC. This results into the conductor entering the thermodynamical Meißner phase. Even further, those conductors show not only the property of an ideal conductor but an ideal diamagnet as well, which is known as the Meißner-Ochsenfeld effect. After these discoveries in the first half of the 20th century, in 1957 the so called BCS theory (named after John Bardeen, Leon Neil Cooper and John Robert Schrieffer) gave a microscopic explanation for superconductivity by postulating a correlated quantum state between two electrons in the conduction band of the material. Those so called Cooper pairs would therefore only form for (very) low temperatures and due to their nature as bosons eventually lead to a vanishing electrical resistance in the material. Important hereby is that this full disappearance only applies to DC, an alternating current is only associated with a greatly reduced resistance. This is due to the property that, simply stated, Cooper pairs prefer to form in the 'slipstream' of other electrons and only the formation of this slipstream causes resistance, but not it's flow. Since the field reversal in AC repeatedly interrupts this slipstream, electrical loss occurs.

Even though the Meißner-Ochsenfeld effect claims an ideal diamagnet, an external magnetic field actually decreases exponentially into the superconductors surface

$$B(z) = B_0 e^{-z/\lambda_L} \tag{3}$$

This is described by the London equations and results into a London penetration depth

$$\lambda_L = \sqrt{\frac{m}{\mu_0 q^2 n_s}} \tag{4}$$

where n_s is associated to the number density of charge carriers, m the mass and q the charge of a carrier. In case of the BCS theory, not electrons are assumed as charge carriers but Cooper pairs, so $m = 2m_e$, $q = 2e$ and $n_s = n_e/2$.[Sch04] If λ_L is depending on the depth into the superconductor (as is the case for an oxygen diffusion profile in a niobium cavity, see sec. 3.3), the London penetration depth and magnetic field are connected by a partial differential equation[CG20]

$$\lambda_L^2 B''(z) + 2\lambda_L \lambda_L' B'(z) - B(z) = 0 \tag{5}$$

The discussed properties alone are defining for the class of type I superconductors. Furthermore, elements like the metal of interest, niobium, show as superconductors of type II an additional phase called the Shubnikov phase in direct succession to the Meißner phase. It prevails until a second critical magnetic field H_{c2} (while the temperature still has to be below T_c). This phase is characterized by magnetic flux vertices entering the superconductor (in case an external

magnetic field is applied) which cause the electrical resistance to rise, but cannot be explained by BCS theory.

Now SRF cavities use niobium, which makes them type II superconductors and they are operated at $1.8 - 2\,\mathrm{K}$, which is below the critical temperature for the Meißner phase of $T_c = 9.2\,\mathrm{K}$. The surface resistance R_S consists of two parts

$$R_S = R_{\mathrm{BCS}} + R_{\mathrm{res}} \tag{6}$$

Here R_{BCS} is the surface resistance due to the alternating RF field as explained by BCS theory and shows a decrease for lower temperatures with convergence to zero. On the other hand R_{res} is the so called residual resistance. It is caused by lattice distortions, grain boundaries and in case of an external magnetic field, normal conducting flux vertices in the Shubnikov phase, as discussed above. The latter is especially for cavities the case, where the magnetic field of the accelerating mode penetrates into the cavity wall. Furthermore, R_{res} is temperature independent and it's decrease is target of cavity treatments.[Sch04]

3.3 Mid-T Bake of SRF Cavities

Taking SRF cavities and carrying out so called *heat treatments* under ultra high vacuum (UHV) with them can significantly improve their performance (recognizable by their quality curve). The proximate cause thereby are modifications in the crystallographic structure of the cavity material and the precise recipe of the treatment can be assumed to be crucial for these modifications. Here it should be kept in mind that minor amounts of impurity atoms are present in every real crystal either by production or due to environmental influence afterwards. Aspecially the niobium crystals will oxidize on their surface simply due to air exposure, resulting into three natural layers of oxides: $\mathrm{Nb_2O_5}$ being the uppermost and thickest, NbO and $\mathrm{NbO_2}$ laying underneath, both being collectively referred to as *suboxides*.

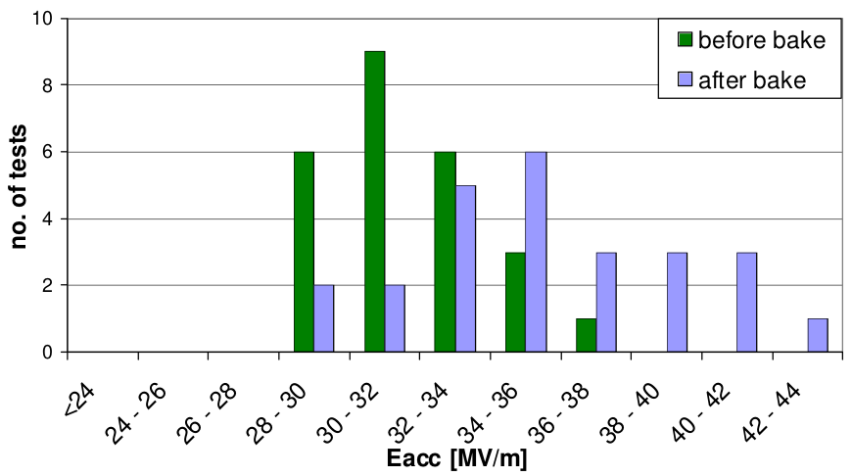

Figure 2: Analysis of maximum E_{acc} for 25 EP treated cavities before and after baking at 100–140 °C, study from 2013 at DESY.[Hao+16]

An instructive plot for the improvements of performing heat treatments for cavities can be seen in fig. 2. In 2019, it was found that by using a new procedure for heat treatments in the temperature range between $200\,^{\circ}\mathrm{C}$ and $400\,^{\circ}\mathrm{C}$ can indeed cause performance improvements.[Pos+19] Because this range lies between lower temperature treatments (like $120\,^{\circ}\mathrm{C}$ for the EuXFEL recipe) and higher temperature treatments above $600\,^{\circ}\mathrm{C}$, those treatments were introduced as the *mid-T heat treatments*. Remarkable about those treatments is, that the temperature is high enough to dissolve the discussed natural oxidation layer and thus oxygen atoms diffuse into the material. Therefore an improvement in performance is observed, not by purifying the cavity, but by impurifying it.

To precisely execute a mid-T treatment you need an oven and four steps consisting of chemical and baking stages. First an electropoliture (EP) is carried out where the cavity is exposed to an acid mixture consisting of hydrofluoric (HF) and sulphuric ($\mathrm{H_2SO_4}$) acid. Followed by a default annealing at $800\,^{\circ}\mathrm{C}$ and afterwards another chemical treatment in form of either another EP or a buffer chemical polishing (BCP) with an acid mixture consisting of HF, nitric ($\mathrm{HNO_3}$) and phosphoric ($\mathrm{H_3PO_4}$) acid. In the latter case, the HF is utilized for the destruction of the $\mathrm{Nb_2O_5}$ layer as in the EP, the $\mathrm{HNO_3}$ serves for regrowing that layer thereafter, meanwhile the $\mathrm{H_3PO_4}$ acts like a buffer due to impurities in the oven. Finally, in the fourth stage the cavity is baked again while temperature and duration are free parameters for the treatment. In case other treatments would be desired, the last stage is customized.

3.4 Principles of Atomic Diffusion

In the considered mid-T treatments, oxygen atoms diffuse into the Nb lattice, which is described primarily by Fickian diffusion. For the substance concentration c (particles per volume, $[c] = \mathrm{m}^{-3}$) and diffusion flux $\vec{\jmath}$ (passing particles per time and area, $[\vec{\jmath}] = \mathrm{s}^{-1}\mathrm{m}^{-2}$), the following equations apply

$$\text{First law:} \quad \vec{\jmath} = -D\nabla c \qquad (7) \qquad\qquad \text{Second law:} \quad \partial_t c = \nabla(D\nabla c) \qquad (8)$$

where D is a diffusion coefficient ($[D] = \mathrm{m}^2\mathrm{s}^{-1}$) and the second law follows directly from the first using the continuity equation. In case of a fixed surface concentration ($c(z=0,t) \equiv c_0 = \mathrm{const.}$), as it applies for oxygen diffusion during mid-T treatments, Fick's second law can be solved *sufficiently* by

$$c(z) = c_0 \,\mathrm{erfc}\left(\frac{z}{\delta}\right) \qquad (9)$$

With erfc the complementary error function[5], c_0 the surface concentration and the depth z. The diffusion length δ is time-dependent and in case of a time-independent diffusion coefficient

[5] $\mathrm{erfc}(x) \equiv 1 - \frac{2}{\sqrt{\pi}} \int_0^x e^{-t^2}\mathrm{d}t$

D given simply by

$$\delta_{\text{hom}} \equiv 2\sqrt{Dt} \tag{10}$$

However in the general case of a treatment $T(t)$ the diffusion coefficient is given by an Arrhenius equation

$$D(T) = D_0\, e^{-\frac{E_a}{k_B T(t)}} \tag{11}$$

and thus time-dependent[Bat+25], which results into the integral

$$\delta_{\text{inhom}} = 2\sqrt{\int_{t_0}^{t_1} D(t)\,\mathrm{d}t} \tag{12}$$

For eq. 11, D_0 is the initial diffusion coefficient and E_a the activation energy, both of which depend on the medium and diffusing particles.

3.5 Theory of EXAFS

Taking a thin foil of some material and radiating photons onto it, results into a transmitted radiation with lower intensity on the other side because of absorption. Plotting the absorption coefficient μ with respect to the photon energy E, we see distinct absorption edges for specific energies (see fig. 3). This is due to the ionization energy of the various bound electrons (meaning the atomic orbitals) to their nucleus in the material – a photon energetic enough to ionize an electron upon interaction will most likely not pass through the foil. Furthermore, a general downwards trend in the absorption can be observed. This can be explained by quantum mechanical reasons, where multiple interaction processes occur and vary in their dominance (see fig. 4).

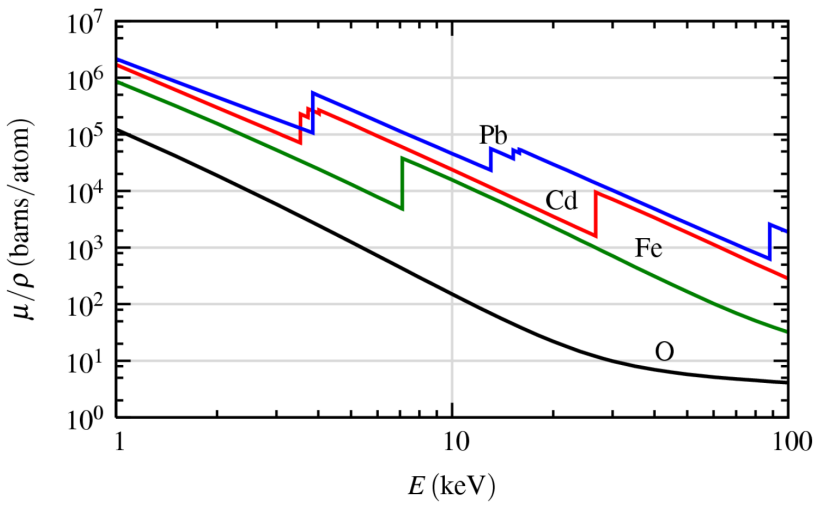

Figure 3: Examples for absorption edges of some chemical elements in a log-log plot for the absorption cross-section over the photon energy.[New04]

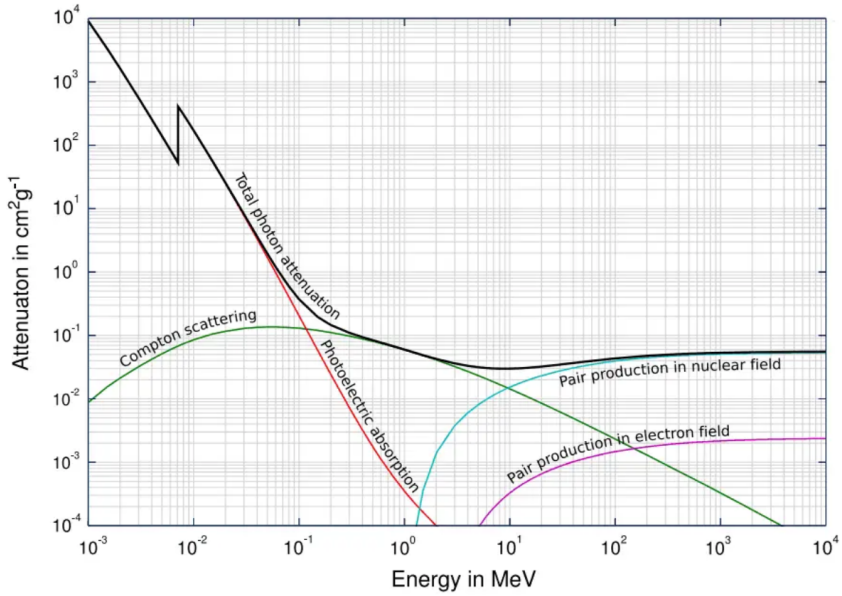

Figure 4: General term of attenuation in an exemplary material as a function of the photon energy. Multiple interaction processes alternate, in EXAFS spectroscopy the photoelectric absorption process is dominating (order of 10^{-2} MeV).

In the 1920s it was first discovered, that above an absorption edge, the absorption curve $\mu(E)$ of a crystallographic solid shows a fine structure with an attenuated trend for increasing energies (see fig. 5). This so called *X-ray absorption fine structure* (XAFS) depends not only on the absorption edge and chemical element, but profoundly on the crystal structure of the foil. It lies in the back scattering processes of the ionized (photo-)electron with bound electrons in the crystal. Expressed in modern (quantum mechanical) terms, the wave function of the electron encountered by a photon, has a pertubated transition between *bound* and *ionized* due to the presence of neighboring (scattering) atoms. This effect can be described quantitatively by a pertubating hamiltonian and application of Fermi's golden rule (utilizing time-dependent pertubation theory). The qualitative explanation hereby can be given by argumenting with resonance conditions inside the absorbing atoms vicinity[6]: When a scattering atom reflects the photo-electron wave function, the initial wave is interfering with the reflecting one and either constructive or destructive interference occurs. In the former case, the transition of *bound to ionized* is favored, while in the latter case it is suppressed. Due to the fixed distance between atoms, the interference changes with increasing energy periodically, which implies a lattice-related oscillation above the absorption edge, as shown in fig. 5. This makes XAFS a non-destructive method for structural analysis of materials.[New04]

The to be analyzed structures in this thesis consist of a bcc lattice of Nb atoms. A major term to investigate lattices is the *j-th coordination sphere*, which describes all atoms in the j-th nearest vicinity of a reference atom (see fig. 6 for the associated *coordination radii*). Additionally an unknown amount of O interstitials in the octahedral void of the lattice is assumed.

[6] *Nachbarschaft* in german.

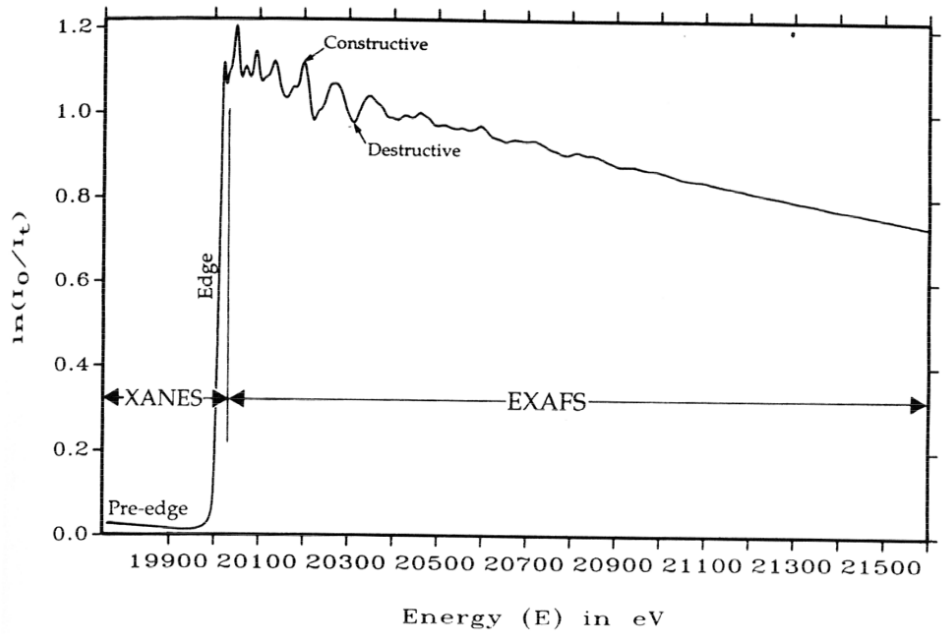

Figure 5: Exemplary XAFS curve (transmittive absorption $\mu(E)$) of the K-edge of molybdenum. The NEXAFS ($\equiv$ XANES) and EXAFS regimes can be distinguished.[Ant]

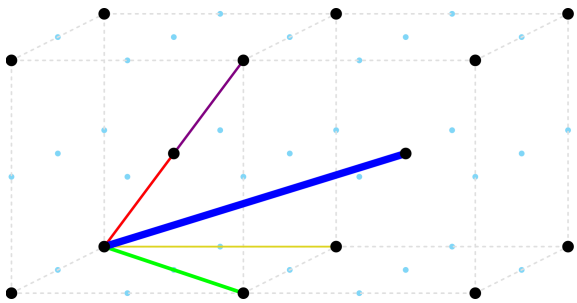

Figure 6: A bcc lattice with the first five coordination radii, the drawn line thickness is a measure for the corresponding coordination number (8, 6, 12, 24 and 8, in ascending order). The positions of the octahedral void are drawn in light blue.

Furthermore XAFS is divided into the *near edge XAFS* (NEXAFS[7]) which applies until about 50 eV and the *extended XAFS* (EXAFS) which follows afterwards. But their boundary is not sharply defined, it consists of the fact that EXAFS is mostly due to single-scattering processes and carries information about the vicinity of an absorbing atom (inter-atomic distances/ lattice constants, coordination numbers/ lattice system, defects, element of neighboring atom) while NEXAFS relies on multiple-scattering processes and contains information about the inner-atomic properties (oxidation state, coordination chemistry, band structure, etc.).[Beh09]

The quantitative approach of EXAFS starts with the following equation:

[7]Synonymous with the historically older term *XANES* (X-ray absorption near edge structure) which is also used in literature.[Bia80]

$$\chi(E) = \frac{\mu(E) - \mu_0(E)}{\Delta\mu_0} \tag{13}$$

χ is called fine structure of the absorption curve μ and furthermore depends on a background function μ_0 and the absorption difference of the absorption edge itself. While there is no full theoretical and quantitative description of the rather complex NEXAFS phenomenon up until today, EXAFS can be understood as a short-range-order phenomenon. This led 1971 to the so called EXAFS equation

$$\chi(k) = \sum_j \frac{N_j\, e^{-2k^2\sigma_j^2}\, e^{-2R_j/\lambda(k)}\, F_j(k)}{kR_j^2} \sin\left(2kR_j + \Phi_j(k)\right) \tag{14}$$

where the fine structure χ is depending on the mean-free-path of the photo-electron $\lambda(k)$, for each coordination sphere j there is a radius R_j, number of neighbors N_j, variance of thermal displacement σ_j^2 and two optical scattering properties $F_j(k)$ (backscattering amplitude) and $\Phi_j(k)$ (backscattering phase).[Lyt00] The wave number of the photo-electron k hereby arises from the non-relativistic quantum mechanical relationship

$$k = \sqrt{\frac{2m_e}{\hbar^2}(E - E_0)} \tag{15}$$

with the photon energy E and edge position E_0.

It can be seen directly from the equation that besides some complicated expression for the amplitude, the EXAFS consists mainly of a linear combination of harmonic oscillations related to the coordination radii. For this reason, performing a fourier transform and considering it's absolute value is standard to obtain R_j as peaks and thus crystallographic information. But caution is advised: The optical phase $\Phi_j(k)$ can be monotonous in k and cause the peaks to be shifted and the optical amplitude $F_j(k)$ can have a local extremum, which leads to a beat[8] in the fine structure and a splitting of two peaks in the fourier space even though they represent only one radius. The latter phenomenon is called Ramsauer-Townsend effect and can be tricky to identify.[Rav12] And in general, a peak that is no perfect gaussian shows side lobes in the fourier space which can be misinterpreted as independent lattice distances.

It is crucial here that the EXAFS analysis in this thesis does not use the transmission of an X-ray beam through a sample, but (due to the thickness of the samples) the fluorencence emitted in it's attenuation. Ionized electrons leave holes which are filled by electrons in higher shells and cause the emission of fluorecence photons. This is a major method for practicing EXAFS spectroscopy, besides measuring the transmission or the direct analysis of Auger electrons. But it goes along with the fact, that in fluorescence only a quantity proportional to the absorption coefficient can be measured. Additionally even the proportionality isn't valid strictly because of the so called *self-absorption*.[Rav11] When a fluorencence photon is emitted (whose probability is actually proportional to the absorptance) it has to travel out through the material again.

[8] *Schwebung* in german.

This process includes secondary absorption of the fluorescence photons and increases for higher primary absorption. Furthermore, the X-ray beams penetration depth into the material (mostly weakly) depends on the photon energy, which results in addition into a varying extent of the self-absorption effect. Thus self-absorption dimms the EXAFS oscillations and leads to a non-linear relationship between transmission and fluoresence EXAFS.

4 Characterization of Sample Treatments

Table 1: Final treatment stage of all three analyzed samples.

Sample N°	Kategory	Treatment	Temperature	Duration
243	mid-T	regular mid-T	300 °C	3 h
245	mid-T	long duration mid-T	250 °C	20 h
247	EuXFEL recipe	low-T baseline	120 °C	48 h

The investigation included the ex situ analysis of three Nb samples with a thickness of 2.8 mm. Each sample has undergone two chemical and two thermal treatments alternately. First a coarse chemistry, followed by a heating up to 800 °C for 3 h and a fine chemistry. Lastly each sample got again heat treated but with individual parameters (see sec. 3.3). Samples 243 and 245 thereby got a mid-T heating and sample 247 was treated with the standard EuXFEL recipe (see tab. 1).

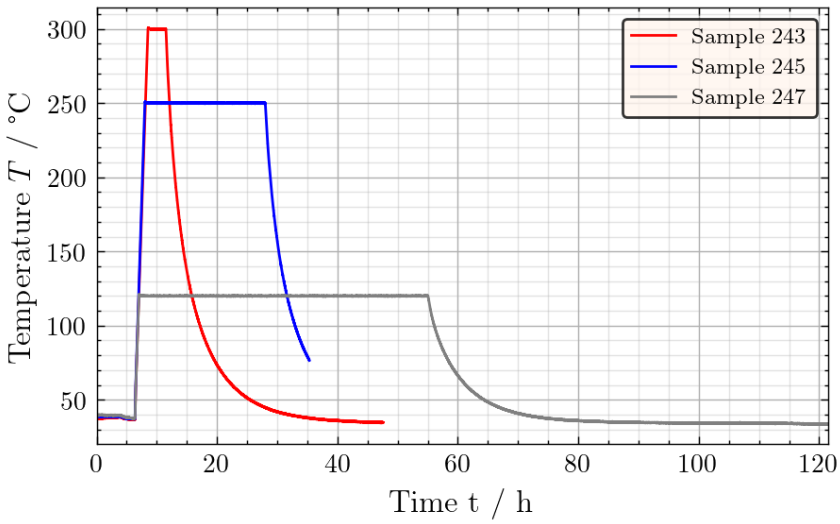

Figure 7: Temperature curve of the final treatment stage of the investigated samples 243 (regular mid-T), 245 (long duration mid-T) and 247 (low-T baseline).

All final stages had a time-dependent temperature $T(t)$, the curves of which are shown in fig. 7. Thus the Fickian diffusion is described by a time-dependent diffusion coefficient $D(t)$ and an integration has to be performed in order to obtain the theoretical diffusion length δ (see eq. 12). Two quantities of the Arrhenius equation (see eq. 11) have to be assumed here, the first is the initial diffusion length $D_0 = 1.5 \cdot 10^{-2}\,\mathrm{cm^2\,s^{-1}}$ and the second is the activation energy $E_a = 1.2\,\mathrm{eV}$. Both values apply for diffusing oxygen in a Nb lattice with some inhomogeneous

influence of grains.[Bat+25] The calculation yields $\delta_{243} = 1442.56\,\mathrm{nm}$, $\delta_{245} = 1102.31\,\mathrm{nm}$ and $\delta_{247} = 20.87\,\mathrm{nm}$ for each sample respectively, whereby it should be noted that δ_{245} is slightly bigger due to the artificial cutoff in the $T(t)$ curve. In reality, the lattice shows distortions like point defects and grain boundaries whose influence is only estimated by the literature values of D_0 and E_a and the material (cavity wall) is relatively thick compared to the diffusion length but not infinite (precisely the diffusion process runs on both sides of the cavity wall, even though one process can be assumed to not affect the other). Thus it is necessary for the diffusion lengths to be checked by the following analysis.

Regarding the purity of the Nb samples in the production process, aspecially tantalum and hydrogen succeeded by some others occur as trace elements. Looking at the atomic percentage of these elements in such a produced niobium ingot yields $257\,\mathrm{ppm\,at.\%}$ for tantalum and $184\,\mathrm{ppm\,at.\%}$ for hydrogen as upper limits, following purity requirements for SRF cavities (other trace elements lie below these concentrations).[Wen15] Comparing this with the atomic percentage of oxygen interstitials due to mid-T treatments, which lies in the order of $\mathrm{at.‰}$ makes one confident that EXAFS will especially not be disturbed by trace elements.

5 Inductive EXAFS Examination of Niobium Samples

The niobium examinations discussed here were carried out at the Dortmund Electron Accelerator (DELTA) which is operated by the Technische Universität Dortmund as a storage ring for electrons. It delivers the needed X-ray radiation as synchrotron radiation of a superconducting wiggler (SCW, see fig. 8). The beamline 8 (BL8) was used, during the period from the 12th to the 16th of May 2025. This beamline is operated by the Bergische Universität Wuppertal and the Nb samples are owned by and were prepared at the MSL group at the Deutsches Elektronensynchrotron (DESY). This way, our experiment represents a tripartite cooperation.

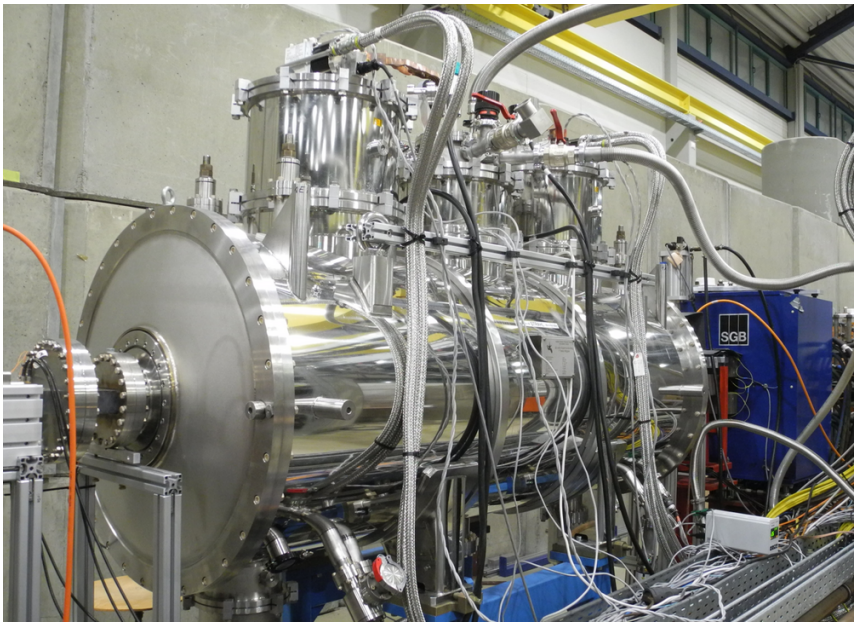

Figure 8: The utilized superconducting wiggler (SCW) provided the used synchrotron radiation through manipulation of $1.5\,\mathrm{GeV}$ electrons in a magnetic field of $7\,\mathrm{T}$ and with a period length of $122\,\mathrm{mm}$ (Source: [Kha]).

5.1 Setup of the Beamline Experiment

The setup of the EXAFS experiment (see fig. 9 respectively 10) is given first by the incoming synchrotron radiation traversing multiple instruments before radiating into the Nb sample, a fraction passing it and traveling through a reference setup and finally to be absorbed by a lead block. Initially there is a crystal pair monochromator consisting of silicon with a piezo element connected to one of the crystals for calibration reasons. This is succeeded by an element for transfering the radiation from the vacuum in the synchrotron into the air. It consists of a Be-window and a Kapton foil, filled with He in between to both ensure the beam quality and keep the vacuum inside the storage ring. Otherwise the Be-window alone would break under the pressure difference.

Subsequently the radiation is passing an aperture $\mathrm{S3}$ and an ionization chamber to measure the initial X-ray intensity I_0. Directly afterwards the Nb sample is attached on a sample mount which in turn is placed on a table. The sample has the shape of a truncated cone and is rotated by an angle θ at it's geometric center (perpendicular to the plane of projection in fig. 9). Above the sample, a detector consisting of silicon called *PIPS* (passivated implanted planar silicon) is capturing the fluorescent photons emitted in the sample in a widespread solid angle. Thus the Nb sample is measured in fluorescence.

Due to the beam diameter, part of the radiation passes by the sample and travels through another aperture $\mathrm{S4}$. After that again an ionization chamber I_1 is installed followed by a reference sample and a third ionization chamber I_2 measuring the reference sample in transmission. At the end, a lead block absorbs the remaining radiation.

5.2 Acquisition of Measurement Spectra

The sample of interest was first fixed to the mount and placed on the table in the setup. Then a calibration process was undertaken, involving the position of the table height and the angle θ of the mount. The beam intensity behind the sample I_1 was plotted against the table height, which results into a logistic-like curve, between the adjustments where the beam passes completely past the sample and where it is completely blocked by it. The turning point of this plot was then set as the calibrated table height. Afterwards, the angle θ was varied and I_1 plotted against θ. Here we got a triangular function, where I_1 is at maximum when the sample is completely parallel to the beam. The maximum point was chosen for θ and defined as zero. After this procedure, the data aquisition was run. For eight different angles

$$\theta \in \{0.1,\ 0.15,\ 0.17,\ 0.2,\ 0.3,\ 0.5,\ 0.7,\ 1\}^\circ$$

the beam energy was varied between $18.837\,\mathrm{keV}$ and $19.407\,\mathrm{keV}$. The energy step between consecutive datapoints and the integration time were chosen separately on four intervals (see tab. 2). The beginning and ending of each scan was of rather little interest, while the intermediate energies carried the more decisive information. The intensities I_0 and PIPS were measured, together with I_1 and I_2. Such a single *exafsscan* on an energy range of $570\,\mathrm{eV}$ took about $23\,\mathrm{min}$.

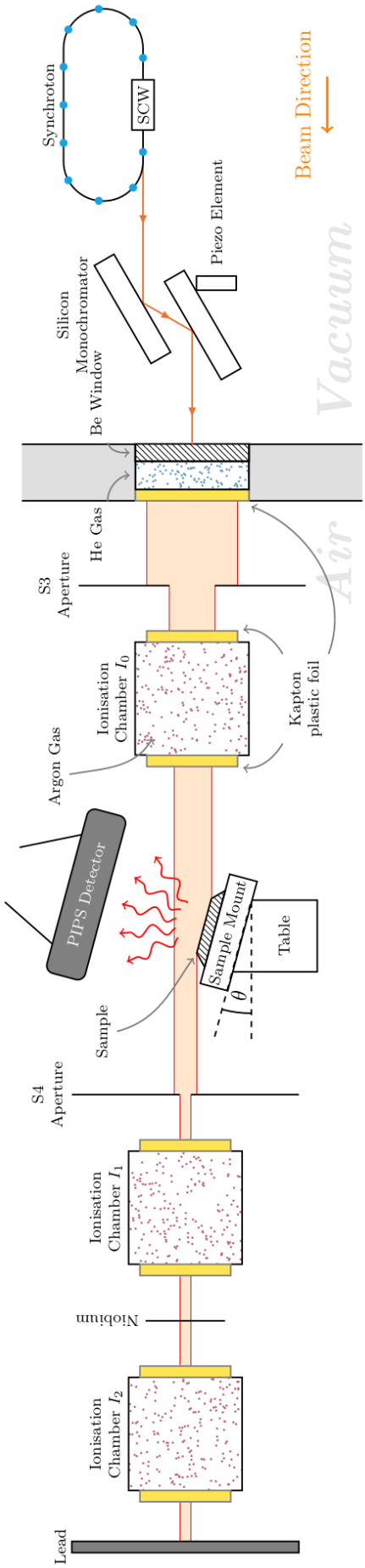

Figure 9: Experimental setup as described in the text. The synchrotron beam is drawn two dimensional after the vacuum-air transition, beam width and distances are not to scale. The author of the graphic is Ivo Ziesche, Friedrich-Schiller-Universität Jena (see Acknowledgements, last page).

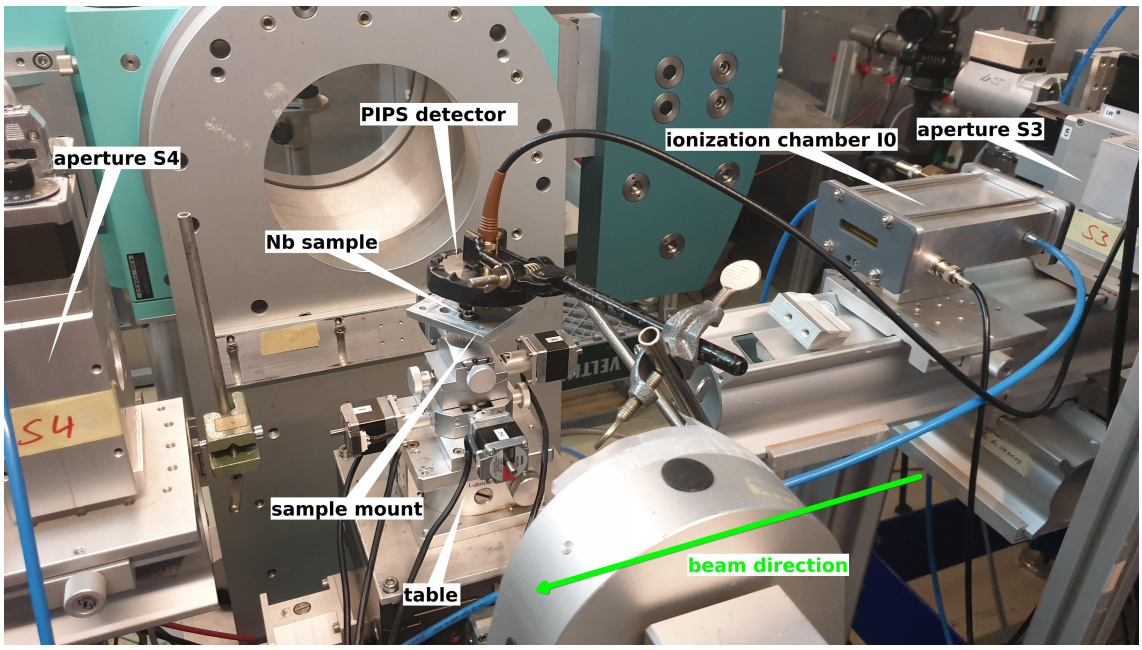

Figure 10: Photograph of the experimental setup.

Between *exafsscans* of this kind, the piezo element of the monochromator was usually used for recalibration by varying the piezo voltage and comparing this with the intensity I_0. The piezo voltage was set to where I_0 is at it's maximum. This ensured, that the monochromator crystals remained aligned parallel to each other.

After the scan of all angles θ the samples were switched and the setup again calibrated. Each setting for sample and angle was measured redundantly multiple times and at different times of day. The procedure was supervised by living beings during the day (between about $8\,\mathrm{AM}$ and $11\,\mathrm{PM}$) and executed automatically by terminal commands during the night.

Each ionization chamber was filled with argon at a pressure of $1\,\mathrm{bar}$, which resulted into about $18\,\%$ of the transmitting radiation to be absorbed. As for all ionization chambers, the electrons and ions of ionized argon atoms travel to the electrodes and cause an electrical current (in the order of nA). Next, a current amplifier converts this current into a voltage, normalized to $10\,\mathrm{V}$ at full scale[9] of the amplifier and a voltage-to-frequency converter transcribes the signal into a rectangular pulse. Electronically, a software counts the pulses, which finally represent the photon counts. The PIPS detector on the other side, detects radiation by them producting electron-hole pairs in the detector, which results into a current that is measured.

5.3 Extracting the Fine Structure

The raw spectrum of a scan is given by the quotient $\mu(E) = \mathrm{PIPS}(E)/I_0(E)$. It is then further processed using the software Athena, which is part of the Demeter package.[RN05][10] It's purpose is to extract the fine structures $\chi(k)$ out of the raw measurements $\mu(E)$ and perform

[9] *Vollausschlag* in german.

[10] Demeter is a software package for the data processing and analysis in the field of x-ray absorption spectroscopy (XAS), where XAFS is a subfield of XAS. It uses the library IFEFFIT for computations.

Table 2: Details of the aquisition of an *exafsscan*. The relative information refers to the K edge of niobium at 18.9855 keV.

Interval	Relative interval	# Datapoints	Step	Integration time
$[18.837, 18.957]$ keV	$[-150, -30]$ eV	40	3 eV	1 s
$[18.957, 19.047]$ keV	$[-30, 60]$ eV	180	0.5 eV	2 s
$[19.047, 19.137]$ keV	$[60, 150]$ eV	120	0.75 eV	3 s
$[19.137, 19.407]$ keV	$[150, 420]$ eV	150	1.8 eV	4 s

a specific fourier transform $|\tilde{\chi}(R)|$ for gaining spacial information. This extraction method ($\mu(E) \to \chi(k), |\tilde{\chi}(R)|$) is standard in the XAFS field and well documented, e.g. in the Athena documentation.[11]

First, poor spectra (high noise level, systematic errors, etc.) are sorted out (see tab. 4 in appendix) and apparent glitches in the remaining spectra are removed (see sec. 8.1). Afterwards, both the edge position E_0 and pre-edge and post-edge lines are fitted into each spectrum. The former is defined by the the first maximum of the first derivative (difference quotient of the discrete data), while the latter are determined by polynomial regression in manually chosen ranges before and after E_0. The pre-edge lines are linear regression curves while the post-edge lines are mostly cubic polynomials (otherwise quadratic, choice was made manually depending on best suitability[12]). The ranges were chosen, so that in the pre-edge region no significant rise in $\mu(E)$ occured due to the absorption edge and no distorting effect of noise appeared. And similarly the post-edge region was selected up to the point where significant noise occured.

Subtracting those regression curves from the pre-edge and post-edge parts of each spectra and normalizing it, provides us a standardized form for each absorption curve, whatever the individual conditions were in the experiment. Then the redundant spectra for the same sample and angle of incidence are averaged and a background curve is calculated, whose difference to the averaged spectrum after the edge corresponds to the fine structure $\chi(E)$ (and thus $\chi(k)$). This background curve is the result of the Athena-intern `AUTOBK` algorithm that uses multiple parameters to compute a spline function, mathematically spoken it shall consist of the lowest frequencies of the absorption spectrum.[13] Also a k-weighting is being done. The exponent chosen depends in general on the shape of the data, here a quadratic weight is used so $k^2\chi(k)$ is considered. The purpose of k-weighting is to mathematically compensate the attenuation of the fine structure amplitude, which can be observed in every empirically EXAFS (seen later in fig. 11) and motivated with the $\frac{1}{k}$ factor in the EXAFS equation (see eq. 14). The chosen exponent however doesn't necessarily need to be 1, because main goal is an overall constant amplitude of the EXAFS, so that a linear combination of non-attenuating oscillations (as expected for distinct atoms in real space) can be analyzed. Instead, even a slightly higher weighting can be beneficial in order to damp the influence of low k fine structure which is part of NEXAFS and not EXAFS. Besides that, because of the measuring in fluorescence, a

[11] See https://bruceravel.github.io/demeter/documents/Athena/index.html

[12] The differences between quadratic and cubic order weren't significant for the needed regressions whatsoever.

[13] The `rbkg` parameter was set uniformly to 1 and the `spline clamps` were set to *None* for `low` and *Strong* for `high`. They influence how strictly the background function follows the absorption curve.

correction of the self-absorption (see sec. 3.5) is performed, because it cannot be eliminated by measurement devices, only corrected artificially.
Therefore another ATHENA-intern algorithm[14], which uses tabulated data for an approximation, is applied.

Finally the fourier transform provides information used for structural deductions. For this the already weighted fine structure $k^2\chi(k)$ is additionally weighted by a *Hanning* window in the range $[1, 10.5]\,\text{Å}^{-1}$ (so called *fourier range*). This helps to further reduce the fine structure of the NEXAFS area we're not interested in. After applying a discrete fourier transformation, we get $|\tilde{\chi}(R)|$.

5.4 Results

The measured spectra show similar behaviour for different angles of the same sample (see fig. 11), aspecially sample 245 shows little changes, as does sample 247, whereas sample 243 exhibits the strongest fluctuations with the angle θ. At about $345\,\text{eV}$, we see a feature for both mid-T treated samples which decreases for higher θ. It doesn't show up for the EuXFEL sample. There is no shift in the edge position identifiable and we see, as expected, a stronger noise level for higher energies/ wavenumbers. In R space the measurements show a strong and broad peak at about $2.6\,\text{Å}$ (see fig. 12). Also some peaks at higher and lower radii seem characteristic. A look onto the measured reference spectra shows no distortions and gives confidence that no fundamental malfunctions occured while beam time.

For further evaluation, a conversion of angles of incidence θ into corresponding penetration depths $z_{1/e}$ (depth up to an attenuation of $1/e$) is helpful, so a more solid state related analysis can be done. The underlying formula[Par54] is a result of electromagnetic optics applied particularly to the X-ray range and given by

$$z_{1/e} = \frac{\lambda}{\sqrt{2}\pi}\left[\sqrt{(\theta^2-\theta_c^2)^2+4\beta^2}-(\theta^2-\theta_c^2)\right]^{-1/2} \tag{16}$$

where the critical angle of incidence θ_c is given approximately by $\theta_c \approx \sqrt{2\delta}$ and the photon wavelength λ only depends on the photon energy E. The optical parameters δ and β are connected to the real and imaginary part of the complex refractive index n of a given medium (defined as $n = 1-\delta+i\beta$). They depend on the lattice type and energy and were taken from the database of the Center for X-ray Optics (CXRO).[15] We obtain a relationship as shown in fig. 13.

As to be assumed, $z_{1/e}$ rises for steeper θ. The penetration depth is actually a function of the photon energy but due to it's low dependence after the absorption edge, a mapping between θ and $z_{1/e}$ can be done. For this, the mean value of $z_{1/e}$ beyond the K edge is chosen.

This allows to further classify the peaks in fig. 12. First 6 different peaks are defined by a local maximum in 6 specific ranges (see tab. 3). Additionally, the peaks width is calculated by the

[14] The algorithm `Fluo` is used, the documentation can be accessed under https://www3.aps.anl.gov/haskel/FLUO/Fluo-manual.pdf.
[15] See https://henke.lbl.gov/optical_constants/getdb2.html

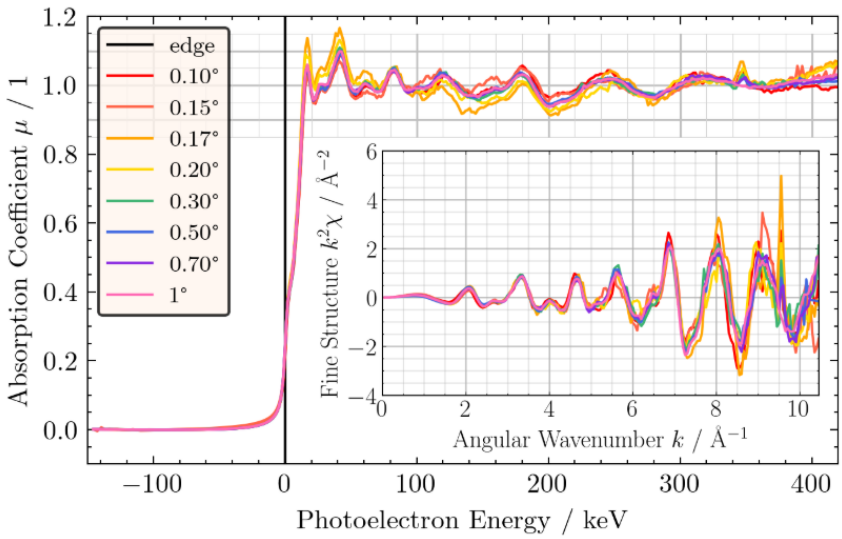

(a) Sample 243

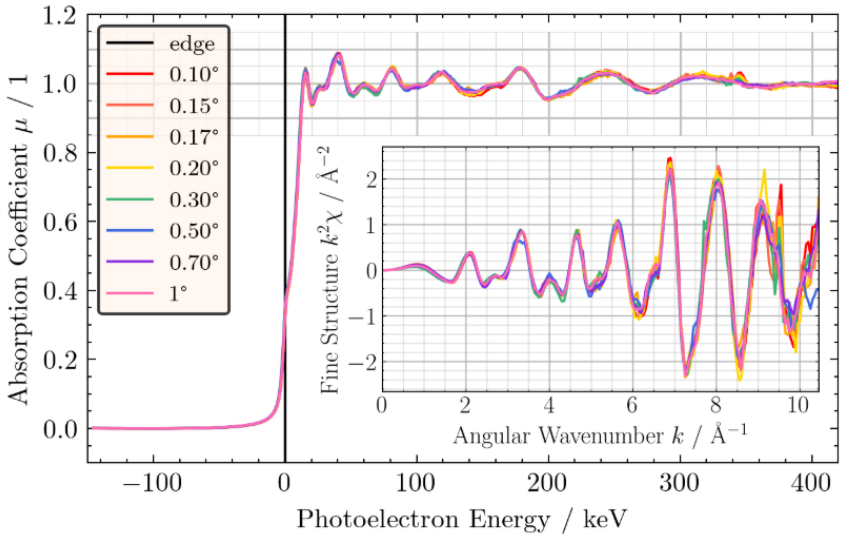

(b) Sample 245

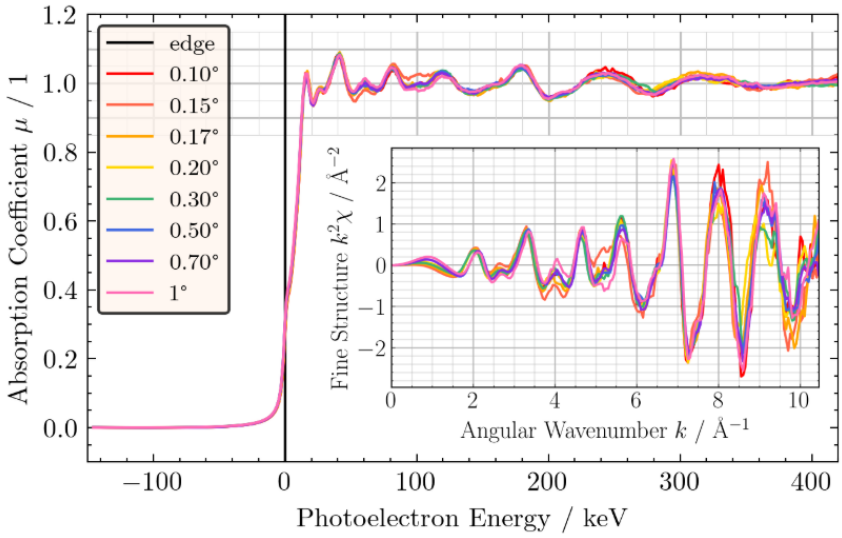

(c) Sample 247

Figure 11: Normalized absorption curves for each analyzed sample and angle of incidence θ. The abscissa was calibrated to the absorption edge, so it indicates the energy of the ionized photoelectron. In addition, the fine structure (EXAFS) of each spectrum weighted by k^2, is plotted.

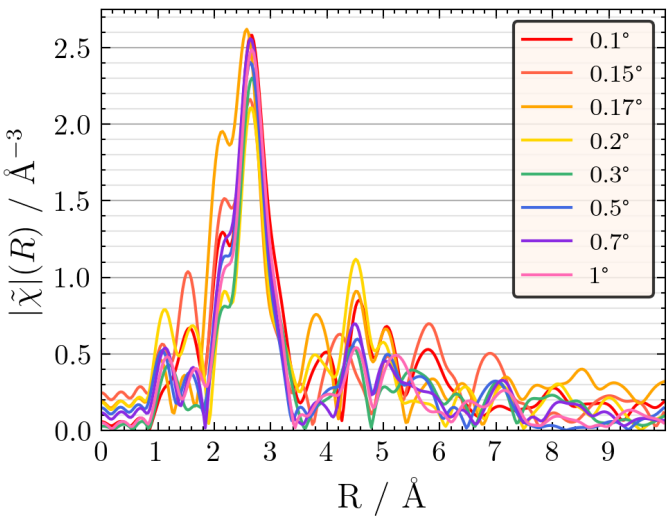

(a) Sample 243

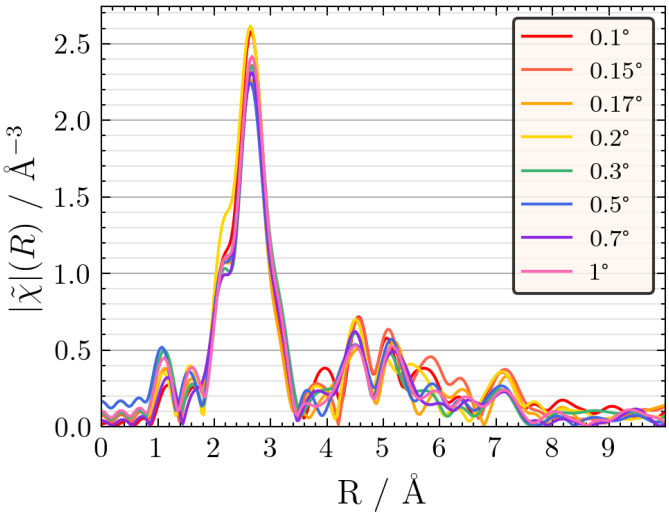

(b) Sample 245

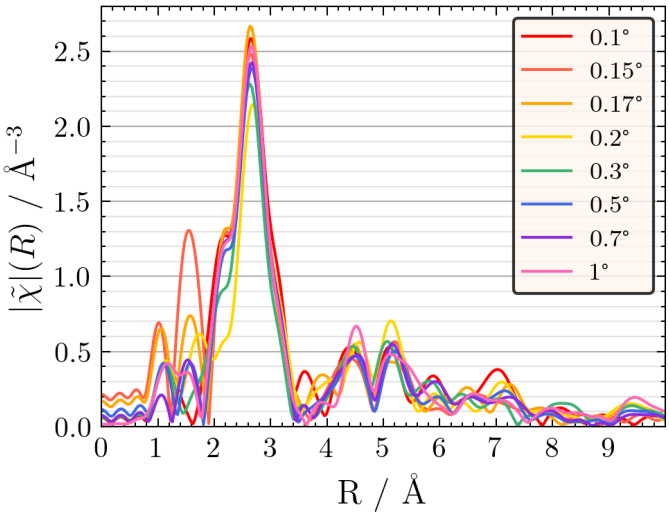

(c) Sample 247

Figure 12: Sample measurements in R space of the spectra shown in fig. 11. At about 2.6 Å, every plot shows a strong and broad peak, together with less distinct but additional peaks.

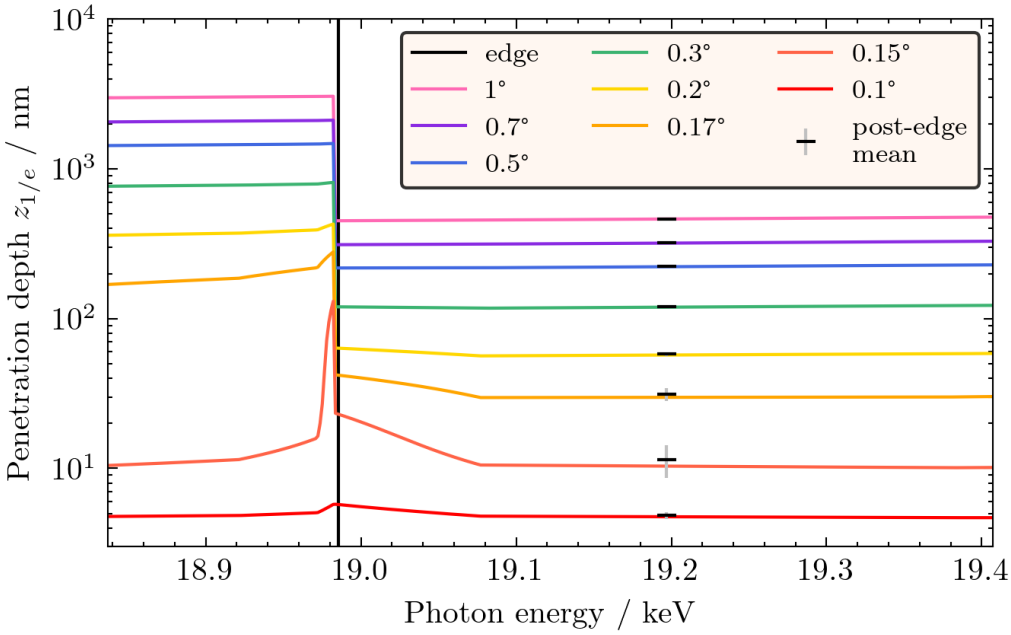

Figure 13: Penetration depth into a pure Nb lattice as a function of the used X-ray radiation energy, calculated after eq. 16. The behaviour of $z_{1/e}$ is approximately constant beyond the K edge, it's mean value and standard deviation is calculated for each angle of incidence. Optical parameters δ, β for calculation were taken from the CXRO database, because the database only stores discrete values, the plot looks edgy.

distance of the turning points before and after that peak.[16] In fig. 14 the identified peaks are plotted together with the assigned penetration depths as discussed.

Table 3: Definition ranges and identification of peaks in the R space measurements.

Peak no.	definition range	identification
1	$[0.9, 1.4]$ Å	1. Nb – O distance
2	$[1.4, 2.0]$ Å	2. Nb – O distance
3	$[2.5, 3.0]$ Å	1. coordination radius (Nb – Nb)
4	$[4.2, 4.8]$ Å	3. coordination radius (Nb – Nb)
5	$[4.8, 5.4]$ Å	4. coordination radius (Nb – Nb)
6	$[6.8, 7.4]$ Å	5. coordination radius (Nb – Nb)

It has to be kept in mind that the R space of a fine structure does not show the radial distribution function inside the sample lattice.[Rav12] Instead the backscattering phase Φ_j of a reflecting atom can shift a peaks position and the backscattering amplitude F_j can cause the Ramsauer-Townsend effect where additional peaks occur without representing real lattice distances (see sec. 3.5). Also, measurement uncertainties and thermal fluctuations inside the lattice can lead to broader peaks, thus a bigger peak may swallow a smaller one. And in general, the fourier transform of a peak will produce multiple peaks as side lobes of that main peak, not representing independent lattice distances themselves.

[16] Points where the second difference quotient of the discrete data has a change of sign.

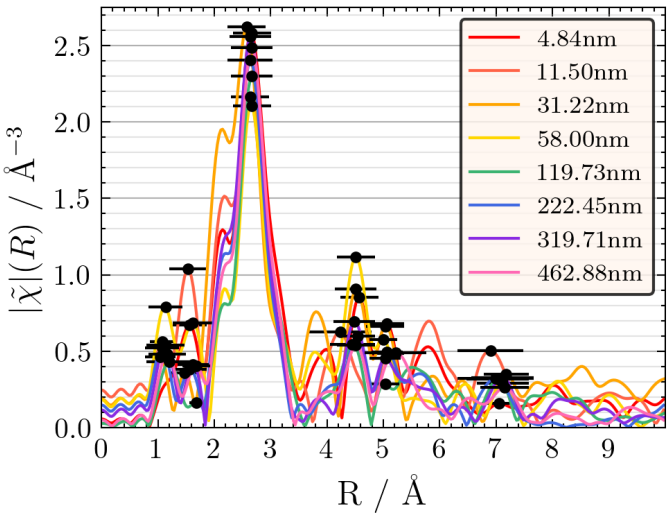

(a) Samples 243

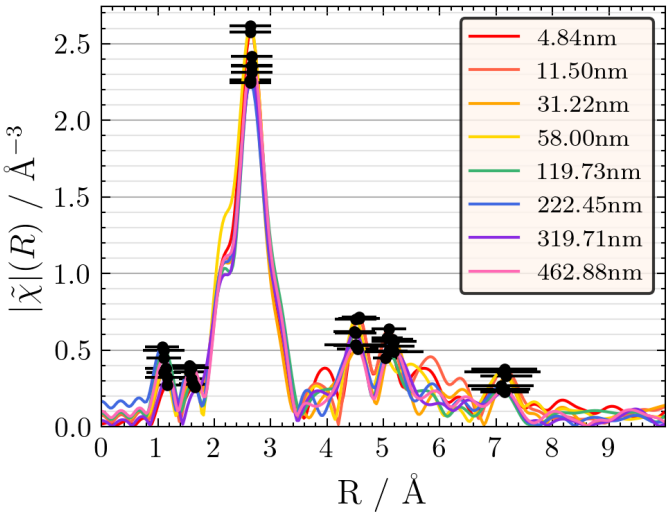

(b) Samples 245

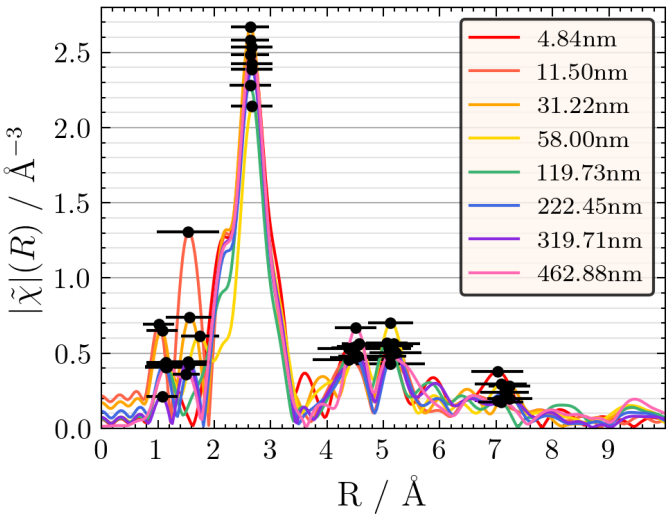

(c) Samples 247

Figure 14: Identification of 6 characteristic peaks in the R space of the measurements, defined as in tab. 3. Their positions, amplitudes and widths are marked. The width of a peak is defined mathematically as the distance between the turning points next to that peak. The angles of incidence have been mapped to penetrations depths following eq. 16.

But an assignment can be done and a comparison with previous analyses allows to identify the coordination shells and characteristic lattice distances.[Kla+20] That way, the marked peaks in the measurements show two $\mathrm{Nb}-\mathrm{O}$ distances and the first, third, fourth and fifth coordination radii. The second coordination radius is not visible, because it is merged into the main peak of the first coordination radius, but the suspicious looking feature left to the main peak on the other hand is uncharacteristic; it is a side lobe of the first coordination radius.

Furthermore the peak migration was analyzed, meaning the changes in position, amplitude and width for varying penetration depths. This is of interest, because changes in the crystal structure imply changes in the position (expanding and contracting lattice) and amplitude (amount of atoms in that vicinity) of peaks in $|\tilde{\chi}|$. The results are displayed in app. B and show mainly insignificant and chaotic behaviour. However the amplitude related to the second $\mathrm{Nb}-\mathrm{O}$ distance shows a distinct attenuation for increasing depth in agreement with the assumption of a decreasing concentration of O interstitials (see fig. 17b). Due to the original normalization of the spectra, only a fitting of a concentration distribution can be accomplished, without any statement regarding quantity.
In fig. 15, those fits are shown. The underlying model is a complementary error function (see sec. 3.4) with the surface concentration c_0, diffusion length δ and an offset as parameters. The data for sample 245 shows no significant trend for a concentration curve to fit to, while sample 243 and 247 do, the former with a greater diffusion length ($\delta \approx 73.69\,\mathrm{nm}$) than the latter ($\delta \approx 44.56\,\mathrm{nm}$).

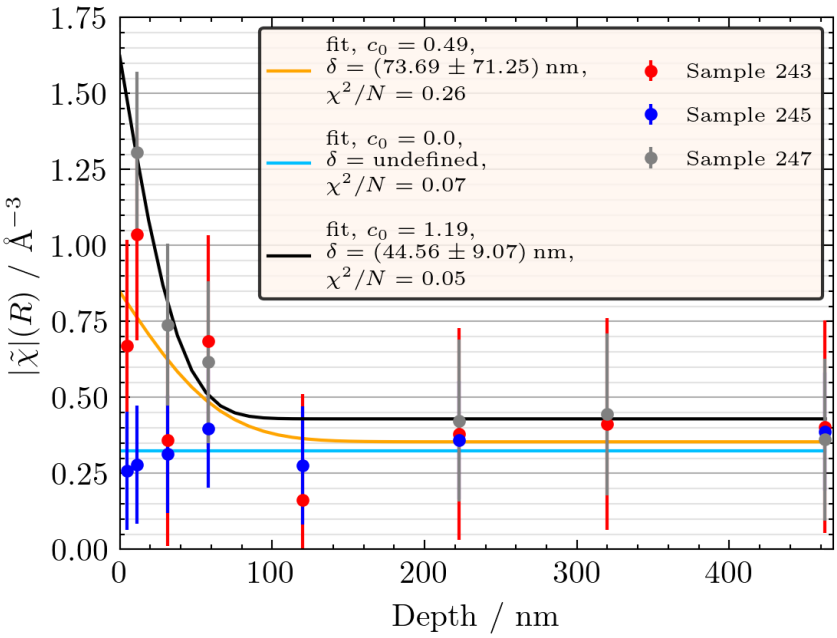

Figure 15: Least squares fit of an interstitial concentration profile to the amplitude behaviour of the 2. $\mathrm{Nb}-\mathrm{O}$ distance (see. fig. 17b), the measurements for sample 245 show no significance for a concentration profile. The fitting function is a complementary error function as described in sec. 3.4. The error bars have a uniform value for each sample respectively (calculated following sec. 6). All χ^2/N values are way below 1.

6 Error Analysis in XAFS

Researchers in the field of XAFS spectroscopy have a special relationship to the estimation of measurement uncertainties. Often uncertainties aren't extimated at all, and when they are, many researchers are showing skepticism whether uncertainties got calculated properly and with the correct method.[BH09] This seems to be due to the highly context-dependent evaluation of XAFS data (see sec. 3.5). Taking the EXAFS equation following eq. 14, it has in case of one considered coordination sphere alone 6 different parameters to be measured/ fitted. This amount of degrees of freedom typically has to be reduced by context-related assumptions, like a crystal lattice and atomic properties (e.g. in the case of this thesis, a bcc lattice of Nb and O as an unknown amount of interstitials). In contrast, other analyses make different assumptions, e.g. for the thermal displacements σ_j or the mean-free-path of the photo-electron $\lambda(k)$, thus the type of information an EXAFS measurement delivers, varies from analysis to analysis. With that the starting point for an error analysis is fluent and thus an universal convention is missing (yet).

Nevertheless, methods for estimating uncertainties exist and vary in their level of detail. First of all, it can be assumed that the energy resolution δE[17] fulfills the proportionality $\delta E = WE$ where $W = 7 \cdot 10^{-4}$ is the fractional energy resolution in a rough estimate, following [MSN81][18]. With regard to eq. 15 and by applying the definition of the total differential, the resolution δk can be obtained by

$$\delta k = \frac{kEW}{2(E - E_0)} \tag{17}$$

Transfering into the R space, in the scope of this thesis, the uncertainty of the radius δR is approximated by the simple relation

$$\delta R = \frac{\pi}{2k_{\max}} \tag{18}$$

with $k_{\max} = 10.5\,\text{Å}^{-1}$ for this analysis.

For the fluctuations of χ and $|\tilde{\chi}|$ on the other hand this thesis relies on a paper discussing high-R components of an XAFS spectrum to measure the RMS[19] as an approximation for the uncertainty ε_R of $|\tilde{\chi}|$.[NBS99] The reason is that those components are equivalent to frequencies that are beyond structural information and only consist of noise. In general it would be appropriate to take components far greater than the farthest identified coordination radius (to avoid structural influence), but due to the small R-range measured, components between $8\,\text{Å}$ and $10\,\text{Å}$ are going to be used, just above the peak of the fifth coordination radius. Furthermore, ε_R can be converted into the uncertainty ε_k of χ by considering Parseval's theorem and assume a k- and R-independence. This leads to the relationship

[17] It should be noted that δE here is not the energy step, but rather the measurement uncertainty.
[18] The paper by Morrison et al. names the double value for W. This is because they discuss the FWHM as δE.
[19] root mean square

$$\varepsilon_k = \varepsilon_R \sqrt{\frac{5\pi}{\delta k \left(k_{\max}^5 - k_{\min}^5\right)}} \tag{19}$$

for a k^2-weighted fine structure, where δk is the resolution of k as introduced and $k_{\min} = 1\,\text{Å}^{-1}$, $k_{\max} = 10.5\,\text{Å}^{-1}$ is the fourier range (see sec. 5.3). The resulting uncertainties δk, ε_k, δR and ε_R are exemplarily plotted in a single curve in appendix C to give a sense of the dimensions of the uncertainties[20].

7 Considerations for EXAFS Simulations

Performing a simulation is helpful in order to rate the possibilities of an EXAFS analysis, but also to verify the consistency of a model on the basis of a well EXAFS measurement. Hereby it is crucial to distinguish between EXAFS measurements in transmission and fluorescence mode. Transmission measurements can be described through the EXAFS equation of Lytle et al. (see eq. 14), while the measurable fluorescence photons intensity suffers from the self-absorption effect and additionally from it's dependence on the X-ray photon energy (penetration depth into the sample depends on the photon energy, see last paragraph in sec. 3.5). This non-linear relationship makes it unsuitable to model fluorescence measurements with the EXAFS equation, even though the spectra look similar. Instead a feasible approach would be to utilize Fresnel theory in order to composite multiple known lattices and calculate their fluoresence EXAFS theoretically. In other words, reference EXAFS spectra of already measured lattices are used to extract optical parameters and simulate a multilayer system whose fluorescence including self-absorption can be calculated. Hereby the strong assumption is made, that a Nb lattice with O interstitials behaves kind of similar to a lattice of niobium suboxides (see sec. 3.3). Because interstitials do not form a lattice but rather lattice defects they cannot be simulated directly and a suboxide lattice has to be approximated for this purpose. Thus such a simulation of fluorescence EXAFS is not suitable for verifying the performed measurement, but rather to investigate similarities in the behaviour of suboxides and O interstitials. The software programs under previous consideration serve this purpose and are therefore unsuitable for simulating an oxygen diffusion profile (see back in introduction, sec. 1).

Simulations of transmission EXAFS (following [New04]) on the other hand, work quite straightforward by first making assumptions for properties of the lattice structure (N, R, σ and edge E_0) and scattering process ($F_j(k)$, $\Phi_j(k)$ and $\lambda(k)$), the latter can be calculated e.g. using the FEFF programm[21]. These can then be inserted directly into the EXAFS equation, where each coordination sphere is represented by an independent summand and a comparison of calculated and measured EXAFS and provides a measure for the similarity of the real lattice to the model (e.g. consisting only of the first two coordination spheres). Multiple of such comparisons can help getting a feeling for the dominant structual parts in the real lattice. Thereby it can be chosen whether this comparison of EXAFS shall be performed in the k space or in the R space.

[20] It is necessary to notice that it seems not clear from Newville et al. ([NBS99]) that a k-weighting of the fluctuation ε_k is needed. I decided to do it anyways in fig. 19, after careful consideration that the errors would otherwise be implausibly small.

[21] See https://monalisa.phys.washington.edu/.

The latter case has the advantage of a direct comparison of single coordination radii where others can be ignored easily, but it requires the complex $\tilde{\chi}$ to compare and not just the absolute value.

8 Discussion of Results and Method

The main result, that sample 243 has a diffusion length of $\delta_{243} = (73.69 \pm 71.25)\,\mathrm{nm}$ and $\delta_{247} = (44.56 \pm 9.07)\,\mathrm{nm}$ for sample 247, tells that the mid-T treated sample 243 indeed shows a higher diffusivity than the EuXFEL reference 247. The obvious explanation hereby is, that the low-T range of 247 is not able to dissolve the natural oxide layer of the niobium surface, thus a lower amount of oxygen atoms diffuse into the material, whereas the mid-T sample 243 fulfills this property, leading to a higher amount of diffusion. Sample 245 on the other hand shows no sign of a diffusion process, which could be explained by a too narrow range of depths chosen for measuring. If the range was chosen wider, an actual profile may be visible in the data, but this would mean that the corresponding diffusion length is way greater than for the other two samples, contradicting the precalculations in sec. 4. Then either the assumption of an erfc-related concentration profile (Fickian diffusion) is wrong, so a deviation of the conventional model is indicated, or the overall interpretation of the peak migration data in fig. 15 is misleading and instead due to strong noise in the measurements.

It has to be concluded, that the measurement uncertainties are way to high to deduce resilient statements about the lattice, as it gets clear by the fact that only one of 18 diagrams of peak migration in app. B was usable for at least some statement.

Performing an EXAFS simulation in fluoresence as considered in sec. 7, would already be possible with the collected data for this thesis. The outcome is not expected to be enlightening, but more like an attempt to get the maximum of what is possible with the available expertise out of the analysis. Since the possiblities of the simulation software programs turned out to not be designed for verifying an EXAFS analysis but rather investigate another academic question.

Compared to the analysis by Luth [Lut24], which only allowed a sight on the white lines[22] of the spectra, to get a rough and indirect estimation for the oxygen concentration, the present thesis allowed more insight. This is due to the application of the fourier transformation and the analysis of the amplitude behaviour.

8.1 Error Discussion

The main source of the measurement uncertainties definitely lies in the low brilliance of the DELTA storage ring and it's wiggler SCW (see sec. 8.3). With this boundary condition and a beamtime of five days, integration time and energy step were chosen accordingly, but 28 of 148 total exafsscans (see app. A) were useless whatsoever and thus due to other reasons. An obvious reason is that construction workers next to the DELTA facility caused vibrations with

[22] The white line of an XAFS spectrum is defined as the first major peak above the absorption edge and thus part of NEXAFS. Because it depends on the inner-atomic distances, interstitial oxygen with a higher electronegativity attract the bound electrons of niobium. Therefore the presence of oxygen interstitials is encoded roughly in the amplitude of the white line.

heavy machinery, strong enough to disturb the experiment during the measurement aquisition, noticable through an oscilloscope. After complaint, they shared their working hours (scheduled aspecially in the morning) with us and we adapted to that, but exceptions occured and made their way as noise into the data. Furthermore, the double crystal monochromator had to be recalibrated ongoingly via the piezo element, to ensure a brilliant beam with a constant intensity and the correct photon energy. Even though it is not plausible to check it strictly, some displacements could have occured because of inaccurate or irregular calibration, which then resulted into systematic errors. Also the measurements during night were vulnerable to disruptions and malfunctions, due to the non-living surveillance. Those exafsscans were checked later by verifing the absorption curves and graph of the electron beam current inside the storage ring. In addition, the synchrotron beam switched multiple times because of reinjections of the electron beam. In the hypothetical case some systematic errors inside the storage ring occured, those could have been in effect only in one electron beam and not the other. But aspecially because almost every exafsscan during the day got repeated during the night and in most cases those measurements were performed with another beam, errors like systematic glitches mostly would have been averaged out. Beyond that, a varying amount of exafsscans was taken redundantly for averaging. This implies a varying fluctuation for averaged spectra and thus influences error estimation, strictly speaking.

Moreover, it can be assumed that many glitches appear in the spectra. One distinct glitch occured in every exafsscan, was located at $+226.1\,\mathrm{eV}$ above the K-edge (or $19\,212.6\,\mathrm{eV}$ as absolute value) and already identified during data aquisition. Possible explanations for this and other glitches in general are defects inside the monochromator crystals (perturbation of Bragg reflection), distortions in other optical instruments (like the kapton plastic foils), incorrect gas composition in the ionization chamber I_0 (which could disturb the intensity measurement $\rightarrow$ lower measured intensity results into a higher calculated absorption coefficient and potentially produces a glitch) or problems inside the synchrotron/ wiggler (some absorbing component manipulating the beam before entering the experimental hut). But apart from the discussed glitch, only a few additional glitches were removed. Aspecially further back in the spectra the data quality was noisy (see fig. 11) and with more experience and courage, the quality could have been improved manually even more. The distinct feature at about $+345\,\mathrm{eV}$ above the K-edge ($19\,330.5\,\mathrm{eV}$ as absolute value), which occurs exactly only in the mid-T treated samples, is suspicious and probably due to the mid-T treatment and not some external disturbance. Regarding roughness considerations, the manufacturing of each samples caused parallel machining marks on the surface during cutting. Trivial considerations beforehand suggested that an alignment of those marks parallel to the beamline reduces effects of roughness in the measurements, but due to forgetfulness this wasn't realized. Instead the approximate orientation of the machining marks on the first mounted sample in the setup was at least kept the same for the other two samples. An alternative influence of roughness are fingerprints and dust which would cause a minor effect in the data. As for the filling gas in the ionization chambers, a proportion of krypton in the argon gas would be imaginable to further increase the intensity measurement and improve the poisson statistics, but due to the about $18\,\%$ absorption in the chambers already, this is a minor consideration.

Looking at the processing procedure afterwards, it would have been possible to set the so called `rbkg` parameter manually for each spectrum, to further optimize background subtraction and thus the extraction of the fine structure, but an uniform value of 1 was chosen instead (see sec. 5.3). Same applies for the `spline clamps`. Regarding the interpretation of the measurements, the surjective character[23] of EXAFS spectroscopy allows multiple conclusions about a feature in the data. Common practice is to take previous analysis of others into account to get to the most plausible interpretation, as it has been done in this thesis as well. Therefore it is worth emphasizing again that this field of spectroscopy relies on this approach. Taking the third and fourth coordination radii for example (see fig. 14), it would be plausible to interpret their peaks in the R space as a Ramsauer-Townsend phenomenon. Only the reference to a previous analysis of Nb lattices, where these peaks were investigated in more detail, makes it clear that they indeed represent independent coordination radii. Same applies for the peak at about $2\,\text{Å}$, which looks appealingly like an independent peak, but is instead a side lobe of the peak next to it.

Furthermore, it is debatable whether the performed error analysis in sec. 6 is appropriate for the performed experiment and it's discussion about SRF cavities in the MSL group. The estimation of δk is already rather detailed compared with the simple approach of defining the energy step as δE and then calculate δk, while δR is simply calculated by the upper fourier range $k_{\max}$ based on the fourier relation and thus expandable. The approach for the χ fluctuation ε_k on the other hand is a bit difficult to rate. On the one side, taking the RMS of the back values of $|\tilde{\chi}|$ in R space turned out empirically to result into the highest estimations for ε_k, compared with the approaches of Poisson counting statistics or taking the direct RMS of the absorption data in the pre-edge or post-edge regimes (following [NBS99]). And because only values in the range between $8\,\text{Å}$ and $10\,\text{Å}$ could be considered, the resulting uncertainty is yet again bigger, which suggests an upper limit. On the other side, assuming a constant[24] ε_k does not acknowledge major glitches or systematic errors (like bad background removal) where a variable uncertainty would be necessary. In these cases the chosen approach cannot represent an upper limit. This can be concluded for ε_R as well due to it's connection to ε_k through the fourier transform, which is the primary uncertainty of interest for this thesis regarding the useful measurements (peak amplitudes, see fig. 15). Without changing the method, ε_R can be improved by measuring a larger range in R space. All in all, the calculated uncertainties proof, that with the available data, a great noise background can be assumed. The χ^2 values in the fittings of fig. 15 are quite low, which often implies an overestimation of uncertainties in the data. In this case on the other hand, it is more plausible that the data suggests a way too low diffusion length due to fluctuations in a rather small depth range. Improving ε_R or enlarging the depth range would help to improve the fits.

[23] By that I mean that multiple crystal structures can look the same in a measurement of the fine structure χ.

[24] With 'constant' is meant that ε_k doesn't depend directly on k. It is indeed depending indirectly on k due to $\delta k(k)$ in eq. 19.

8.2 Methodological Comparison

Besides studying the oxygen concentration profile via EXAFS spectrocopy, other analyzation methods are common and they reveal more about how to look at EXAFS for SRF research and the results of this thesis. LE-μSR (Low energy muon spin rotation spectroscopy) utilizes muons as local magnetic probes, in order to gain information about the magnetic field inside a sample through the muon decay and it's spin disturbance by that local magnetic field. In an investigation of the three samples discussed in this thesis, by Ghanbari et al.[25], their magnetic field distribution was measured and the corresponding oxygen concentration distribution deduced. The preliminary result is that $\delta_{243} = (150.0 \pm 3.4)\,\mathrm{nm}$, $\delta_{247} = (30 \pm 14)\,\mathrm{nm}$ and no plausible value for δ_{245} can be determined. This is consistent with the determined values in fig. 15, where δ_{243} is clearly bigger than δ_{247} and sample 245 shows no significant erfc behaviour. But it seems to be clear as well that the EXAFS analysis did not do well in terms of quantitative accuracy, already due to the large uncertainty of the fit ($\delta_{243} = (73.69 \pm 71.25)\,\mathrm{nm}$ and $\delta_{247} = (44.56 \pm 9.07)\,\mathrm{nm}$). Moreover because the results of Ghanbari et al. can be understood as a lower bound to the true values due to a sensitivity of that method only until about $100\,\mathrm{nm}$ depth. Another approach is the SIMS analysis (secondary ion mass spectrometry) where an ion beam is sputtered onto the sample surface in order to knock out the lattice atoms as *secondary ions*, whose detection is utilized for a statistical analysis of the removed atom counts as a function of depth. Because the natural oxide layers are negligibly thin compared with the diffusion length, the oxygen counts directly give a measure for the interstitial concentration distribution. Significant for this sputtering method is that unlike EXAFS or LE-μSR spectroscopy it is destructive, thus a sample cannot be analyzed twice. A study using *time-of-flight* SIMS by Bate et al. in 2025[Bat+25] found that out of six different mid-T treated samples at least three samples showed strong consistency between the theoretical Fickian diffusion length (see eq. 12) and the SIMS-measured one, while the other three show clearly higher diffusion lengths. A plausible assumption the paper made, are grain boundaries in which the diffusivity is higher than in the lattice. This applies for this thesis too, as already touched in sec. 4. Beyond that, a number of other methods utilizing X-ray diffraction techniques or scanning electron microscopy can also analyze suboxides in cavities, but only poorly oxygen interstitial profiles (see e.g. [Sem+19]).

8.3 Outlook

Further oxygen profile investigations at DELTA are unlikely to yield much better results, it seems the optimum with this machine got reached. The PETRA III facility at DESY on the other hand, provides an enormously higher brilliance, compared to DELTA. While this analysis utilized a brilliance in the order of $10^{15}\,\frac{1}{\mathrm{s\,mrad^2\,mm^2\,0.1\,\%\,BW}}$ at DELTA[26], a possible beamline experiment at PETRA III would have access to an order of $10^{24}\,\frac{1}{\mathrm{s\,mrad^2\,mm^2\,0.1\,\%\,BW}}$![Sch05][Ira06] This would open the gates for a far more comprehensive study, in terms of the amount of analyzable samples, integration time, energy step and angle of incidence settings. The single exafsscan with the parameters in this study within a time of $23\,\mathrm{min}$, would shrink to $1\,\mu\mathrm{s}$. This is a purely

[25] Yet to be published.

[26] This order of magnitude is valid for the superconducting asymmetric wiggler (SAW) at DELTA, the predecessor of the SCW.

mathematical value, because the high brilliance applied to the present setup would smear the photon energies and thus prohibit data aquisition. So an intentional delay of the measurements would be necessary or another setup, like for energy-dispersive EXAFS, which is far beyond the scope of this thesis, could be utilized.

These benefits seem very convincing, but the crucial point here for future projects is, whether EXAFS can actually deliver the desired quantitative results by a raised brilliance or systematic problems in this method rather suggest to focus the ressources on a more reliable method. Due to a missing simulation approach for EXAFS data, it cannot be judged if the measurements follow theoretical considerations in principle and a reliable oxygen concentration profile could be obtained. But previous EXAFS measurements [Kla+20] at PETRA III showed that very distinct fine structures can be resolved and thus confidence in case of oxygen interstitials is justified.

Furthermore the selection of samples can be of interest for future analyses. The intentional focus on only three samples was due to the bad experience with EXAFS measurements at DELTA before. If a higher brilliance is accessible, it will become attractive to analyze more samples again, like aluminium coated samples which serve the purpose of preventing the suboxides to disappear into the vacuum while heating. These resulting oxygen profiles are of great interest as well.

9 Conclusion

This thesis provided an analysis of the oxygen diffusion profile of three differently heat treated samples, two in form of experimental mid-T baking and the remaining one as a reference for the standard low-T baseline baking, utilized in currently operating cavities, installed e.g. in the European XFEL in Hamburg. The measurement of EXAFS at the DELTA facility suffered under high noise levels, thus the quantitative results are not trustworthy and even qualitatively barely statements can be provided. Given that the trend in measurement is not due to random fluctuations, no deviation from the basic Fickian diffusion behaviour could be found and as expected, the regular mid-T treatment results into a higher diffusion length than the EuXFEL recipe. Irritating is the missing outcome for the the second, long duration mid-T treatment, which can most likely be explained by an overshadowed trend due to measurement noise. All in all, we have at maximum a confirmation of the known and beyond that, noise that invites to speculation. This goes hand in hand with the conclusion that more or less the maximum of possibilities at the DELTA facility got provoked. Further interpretation was thus up to the identification of errors. Various noise sources and glitches have been pointed out, from which future EXAFS analyses will benefit. The provided error analysis confirms a wide range of possible results for the concentration profile due to large calculated uncertainties. Hereby the extent of uncertainty estimation allows several different approaches, whereby the overall handling of error determination is generally underdeveloped in the XAFS community. The hope of simulating EXAFS spectra in order to provide a comparison with DELTA measurements, turned out to be inappropriate for the given experiment, upcoming fluoresence analyses with less noisy data could at maximum utilize simulations to focus on the investigation of similarities in the optical behaviour of suboxide layers and oxygen interstitials. In case of a future analysis in transmission mode, EXAFS simulations can actually be used to verify the success of a measurement. The classification of EXAFS in alternative analysis methods, showed that this thesis did not contradict previous analyses, but potential for future investigations utilizing EXAFS exists. The favoured repetition of this investigation at the PETRA III facility at DESY, would enable a far more detailed analysis in terms of sample number, material depth resolution and accuracy.

References

[Ale] D. Alesini. 'LINAC. Introduction to Accelerator Physics'. In: Proc. of the CAS course (). last accessed on 19/10/2025, p. 8. URL: https://arxiv.org/pdf/2103.16500v1.

[Ant] Mark A. Antonio. 'EXAFS. Extended X-Ray Absorption Fine Structure'. In: (), p. 217. URL: https://glass.rutgers.edu/sites/default/files/uploads/virtual/dir.cullity/B-ch%204.2-EXAFS.pdf.

[Aun+00] B. Aune et al. 'Superconducting TESLA cavities'. In: Phys. rev. spec. top. - accelerators and beams 3 (2000). last accessed on 19/10/2025. DOI: 10.1103/PhysRevSTAB.3.092001. URL: https://journals.aps.org/prab/abstract/10.1103/PhysRevSTAB.3.092001.

[Bat+25] Christopher Bate et al. 'Correlation of srf performance to oxygen diffusion length of medium temperature heat treated cavities'. In: Supercond. Sci. Technol. 38 (10th Jan. 2025). last accessed on 19/10/2025. DOI: https://doi.org/10.1088/1361-6668/ad9fe8. URL: https://inspirehep.net/literature/2806599.

[Bau+06] P. Bauer et al. 'A Collection of Selected High Field Q-Slope Studies, Models and Comments. Review of Q-Drop in SRF Cavities'. In: (16th Jan. 2006). last accessed on 19/10/2025, p. 5. URL: https://www.researchgate.net/publication/255591850_A_Collection_of_Selected_High_Field_Q-Slope_Studies_Models_and_Comments.

[Beh09] Malte Behrens. 'Extended X-Ray Absorption Fine Structure'. In: Fritz Haber Institut (Dec. 2009). last accessed on 19/10/2025. URL: https://www.fhi.mpg.de/1073284/malte_behrens__extended_x-ray_absorption_fine_structure__091204.pdf.

[BH09] Corwin H. Booth and Yung-Jin Hu. 'Confirmation of standard error analysis techniques applied to EXAFS using simulations'. In: J. Phys.: Conf. Ser. 190.012028 (2009). last accessed on 19/10/2025, pp. 1–6. DOI: 10.1088/1742-6596/190/1/012028. URL: https://iopscience.iop.org/article/10.1088/1742-6596/190/1/012028.

[Bia80] Antonio Bianconi. 'Surface X-Ray Absorption Spectroscopy: Surface EXAFS and Surface XANES'. In: Applications of Surface Science 6 (3-4 24th Oct. 1980). last accessed on 19/10/2025, pp. 392–418. DOI: https://doi.org/10.1016/0378-5963(80)90024-0. URL: https://www.sciencedirect.com/science/article/abs/pii/0378596380900240.

[CG20] M. Checchin and A. Grassellino. 'High-field Q-slope mitigation due to impurity profile in superconducting radio-frequency cavities'. In: Appl. Phys. Lett 117 (6th July 2020). last accessed on 19/10/2025. DOI: https://doi.org/10.1063/5.0013698. URL: https://inspirehep.net/literature/1795952.

[Hao+16] J. Hao et al. 'Low temperature heat treatment effect on high-field epcavities. Proceedings of the 11th Workshop on RF Superconductivity, Lübeck-/Travemünder, Germany'. In: (2016). last accessed on 19/10/2025, p. 1. URL: https://proceedings.jacow.org/SRF2003/papers/mop16.pdf.

[Ira06] Martashvili Irakli. 'Optimizing the Laser Pulse Shape'. In: (15th Sept. 2006). last accessed on 19/10/2025. URL: https://www.researchgate.net/publication/242169493_Optimizing_the_Laser_Pulse_Shape.

[Kha] Shaukat Khan. 'Supraleitender 7-T-Wiggler SCW'. In: (). URL: https://delta.tu-dortmund.de/forschung/beschleuniger/.

[Kla+20] Jonas Klaes et al. 'High-temperature treatments of niobium underhigh vacuum, dilute air- and nitrogen-atmospheres as investigated by in situ X-ray absorption spectroscopy'. In: J. Synchrotron Rad. 28 (10th June 2020). last accessed on 19/10/2025, pp. 266–276. ISSN: 1600-5775. DOI: https://doi.org/10.1107/S1600577520013557. URL: https://pmc.ncbi.nlm.nih.gov/articles/PMC7842222/.

[Lut24] Lennard Felix Luth. 'Oxygen concentration study in Nb using XAFS'. In: (Nov. 2024), p. 53.

[Lyt00] Farrel W. Lytle. 'The EXAFS family tree: a personal history of the developmentof extended X-ray absorption fine structure'. In: J. Synchrotron Rad. 6 (22nd Jan. 2000). last accessed on 19/10/2025, pp. 123–134. DOI: https://doi.org/10.1107/S0909049599001260. URL: https://journals.iucr.org/paper?S0909049599001260.

[MSN81] Timothy I. Morrison, G. K. Shenoy and Dimitros Niarchos. 'Noise Level and Resolution Effects in EXAFS Spectra'. In: J. Appl. Cryst. 15 (10th Sept. 1981). last accessed on 19/10/2025, pp. 388–390. DOI: 10.1107/S0021889882012229. URL: https://www.researchgate.net/publication/244633695_Noise_level_and_resolution_effects_in_EXAFS_spectra.

[NBS99] Matthew Newville, Boyan I. Boyanov and Dale E Sayers. 'Estimation of uncertainties in X A F S data'. In: J. Synchrotron Rad 6 (June 1999). last accessed on 19/10/2025, pp. 264–265. ISSN: 0909-0495. DOI: 10.1107/S0909049598018147. URL: https://www.researchgate.net/publication/8446879_Estimation_of_uncertainties_in_XAFS_data.

[New04] Matthew Newville. 'Fundamentals of XAFS'. Version 1.6. In: (22nd July 2004). last accessed on 19/10/2025. URL: https://www.lehigh.edu/imi/teched/GlassCSC/SuppReading/Tutorials.pdf.

[Par54] L. G. Parratt. 'Surface Studies of Solids by Total Refiection of X-Rays'. In: Physical Review 95.2 (15th July 1954). last accessed on 20/10/2025, pp. 360–361. DOI: https://doi.org/10.1103/PhysRev.95.359. URL: https://nucssp.rmki.kfki.hu/articles/catalog/54/parratt.pr.95.359.1954.pdf.

[Pos+19] S. Posen et al. 'Ultra-low surface resistance via vacuum heat treatment of superconducting radiofrequency cavities'. In: ResearchGate (July 2019). last accessed on 19/10/2025. DOI: https://doi.org/10.1103/PhysRevApplied.13.014024. URL: https://www.researchgate.net/publication/338590329_Ultralow_Surface_Resistance_via_Vacuum_Heat_Treatment_of_Superconducting_Radio-Frequency_Cavities.

[Rav11] Bruce Ravel. 'Understanding self-absorption in fluorescence XAS'. In: (14th Jan. 2011). last accessed on 19/10/2025. URL: https://speakerdeck.com/bruceravel/understanding-self-absorption-in-fluorescence-xas.

[Rav12] Bruce Ravel. 'The Ramsauer-Townsend effect in EXAFS'. In: (3rd July 2012). last accessed on 19/10/2025. URL: https://speakerdeck.com/bruceravel/the-ramsauer-townsend-effect-in-x-ray-absorption-spectroscopy.

[RN05] Bruce Ravel and Matthew Newville. 'ATHENA, ARTEMIS, HEPHAESTUS: data analysis for X-ray absorption spectroscopy using IFEFFIT'. In: Journal of Synchrotron Radiation 12 (Apr. 2005). last accessed on 19/10/2025, pp. 537–541. DOI: 10.1107/S0909049505012719. URL: https://journals.iucr.org/paper?S0909049505012719.

[Sch04] Peter Schmüser. 'Superconductivity'. In: CAS - CERN accelerator school (11th Sept. 2004). last accessed on 19/10/2025, p. 20. DOI: 10.5170/CERN-2004-008. URL: https://cds.cern.ch/record/503603.

[Sch05] Detlev Schirmer. 'Synchrotron radiation sources at DELTA'. In: (Jan. 2005). last accessed on 19/10/2025. URL: https://delta.tu-dortmund.de/storages/delta/r/Forschung/Maschinelles_Lernen/Publikationen/DELTA-Int-Rep-1-5.pdf.

[Sem+19] G. D. L. Semione et al. 'Niobium near-surface composition during nitrogen infusion relevant for superconducting radio-frequency cavities'. In: PHYSICAL REVIEW ACCELERATOR 22 (31st Oct. 2019). last accessed on 19/10/2025. DOI: https://doi.org/10.1103/PhysRevAccelBeams.22.103102. URL: https://journals.aps.org/prab/abstract/10.1103/PhysRevAccelBeams.22.103102.

[Web08] Jordan Webster. 'High Field Q-slope and Superconducting Radio Frequency Cavity Testing'. In: (4th Aug. 2008). last accessed on 19/10/2025. URL: https://w4.lns.cornell.edu/rsrc/Home/StudentOpportunities/ReuProjects2008/Webster_Paper.pdf.

[Wen15] Marc Wenskat. 'Automated Surface Classification of SRF Cavities for the Investigation of the Influence of Surface Properties onto the Operational Performance'. In: (2015). last accessed on 19/10/2025. URL: https://bib-pubdb1.desy.de/record/221603/files/PhD%20Thesis%20Wenskat.pdf.

A Raw Measurements

Table 4: Overview of collected exafsscans.

Sample	angle θ / °	# total	# total@day	# total@night	# used (& averaged)	# used@day	# used@night	# dismissed	# dismissed@day	# dismissed@night
243	0.1	**7**	4	**3**	4	3	1	3	1	2
	0.15	**8**	5	**3**	3	2	1	5	3	2
	0.17	**7**	4	**3**	4	4	0	3	0	3
	0.2	**8**	3	**5**	3	3	0	5	0	5
	0.3	**5**	3	**2**	4	3	1	1	0	1
	0.5	**4**	3	**1**	4	3	1	0	0	0
	0.7	**4**	3	**1**	4	3	1	0	0	0
	1	**4**	0	**4**	4	0	4	0	0	0
245	0.1	**8**	6	**2**	8	6	2	0	0	0
	0.15	**8**	3	**5**	7	2	5	1	1	0
	0.17	**8**	8	**0**	6	6	0	2	2	0
	0.2	**5**	2	**3**	5	2	3	0	0	0
	0.3	**6**	3	**3**	4	3	1	2	0	2
	0.5	**6**	3	**3**	5	3	2	1	0	1
	0.7	**6**	3	**3**	5	3	2	1	0	1
	1	**4**	1	**3**	4	1	3	0	0	0
247	0.1	**6**	3	**3**	6	3	3	0	0	0
	0.15	**7**	3	**4**	6	2	4	1	1	0
	0.17	**7**	3	**4**	7	3	4	0	0	0
	0.2	**6**	3	**3**	6	3	3	0	0	0
	0.3	**6**	4	**2**	6	4	2	0	0	0
	0.5	**6**	4	**2**	6	4	2	0	0	0
	0.7	**6**	4	**2**	5	3	2	1	1	0
	1	**6**	1	**5**	4	0	4	2	1	1

B Peak Migration

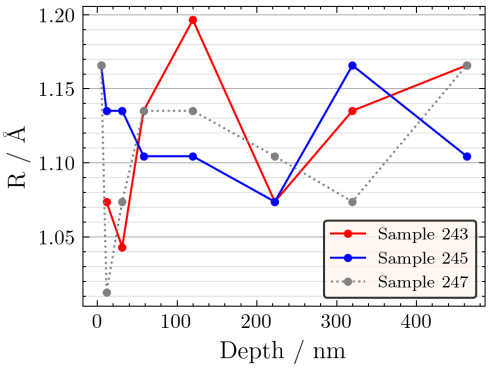

(a) 1. Nb – O distance

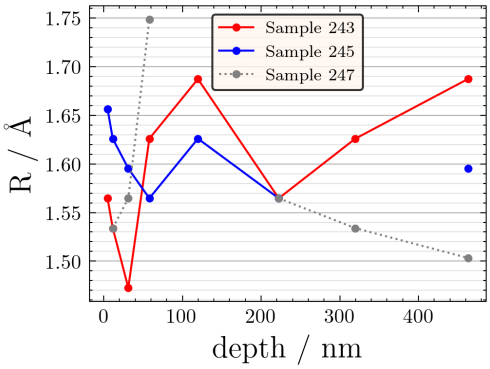

(b) 2. Nb – O distance

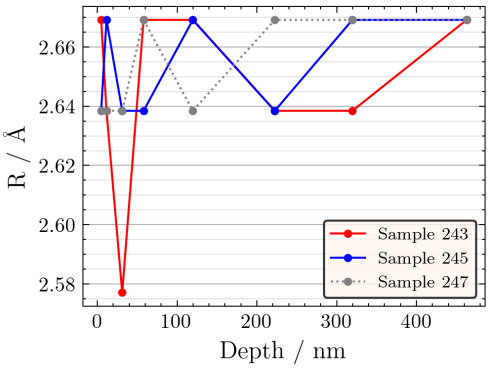

(c) 1. coordination radius (Nb – Nb)

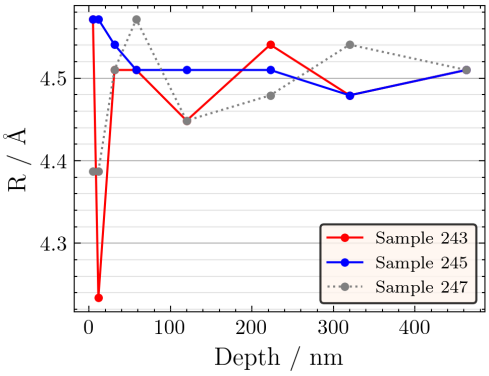

(d) 3. coordination radius (Nb – Nb)

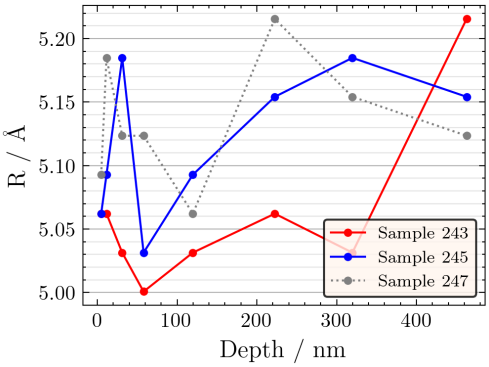

(e) 4. coordination radius (Nb – Nb)

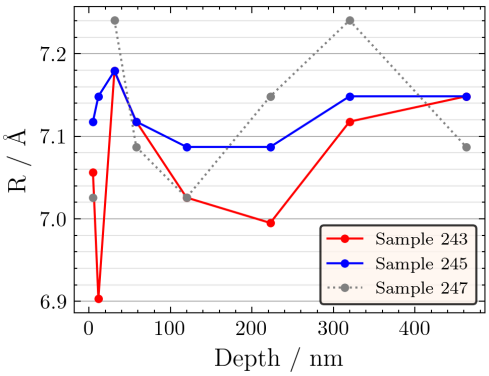

(f) 5. coordination radius (Nb – Nb)

Figure 16: Peak position (and thus, to a certain extent, lattice distances) as a function of the penetration depth. The lines are for illustrative purposes only and do not represent data, same applies for fig. 17 and 18.

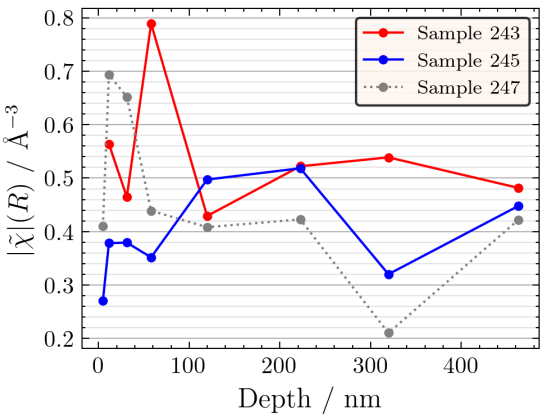

(a) 1. Nb – O distance

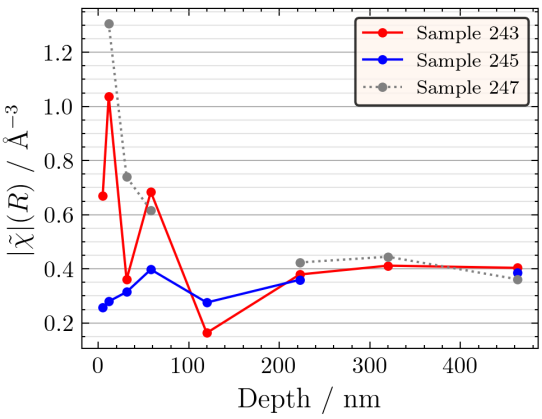

(b) 2. Nb – O distance

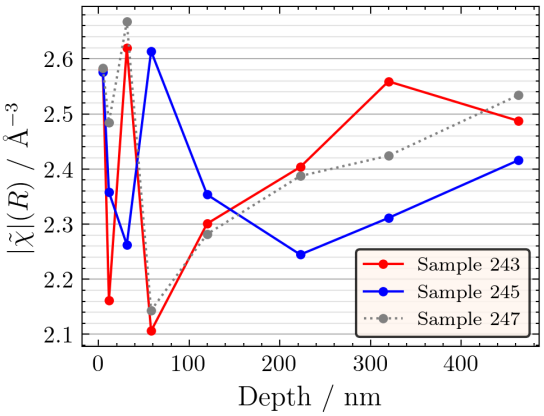

(c) 1. coordination radius (Nb – Nb)

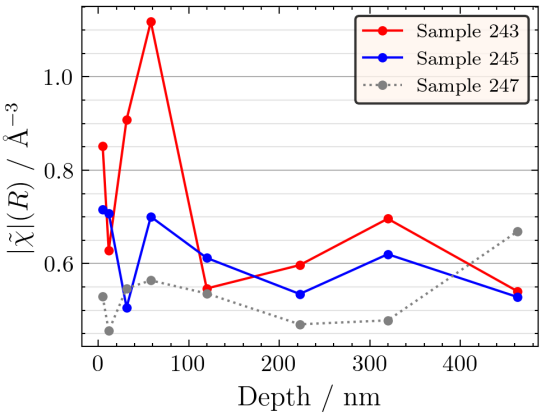

(d) 3. coordination radius (Nb – Nb)

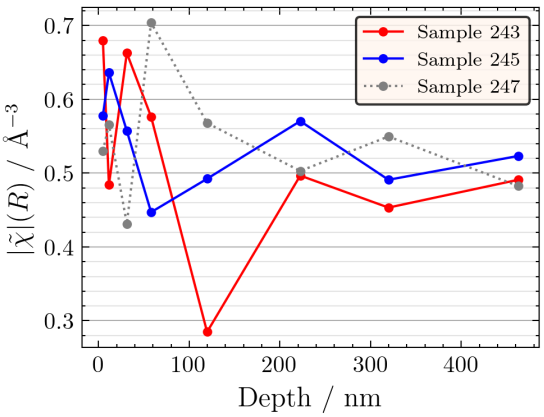

(e) 4. coordination radius (Nb – Nb)

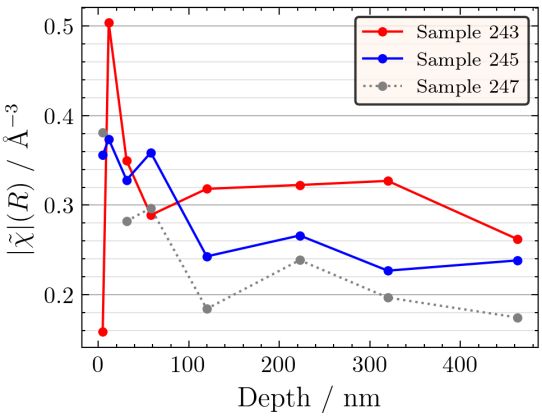

(f) 5. coordination radius (Nb – Nb)

Figure 17: Peak amplitude as a function of the penetration depth.

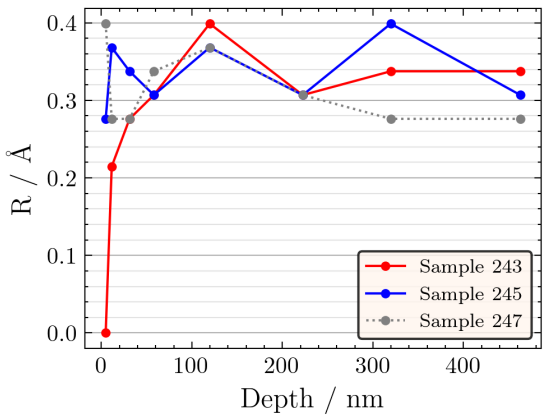

(a) 1. Nb – O distance

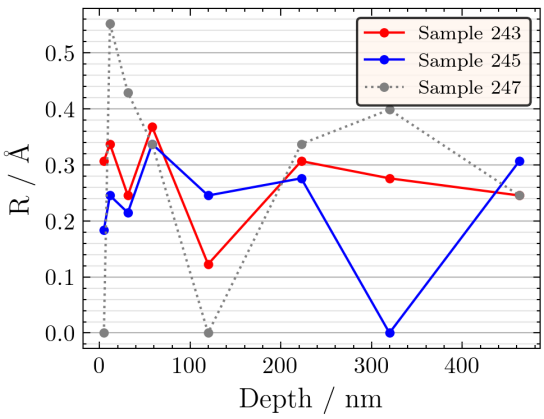

(b) 2. Nb – O distance

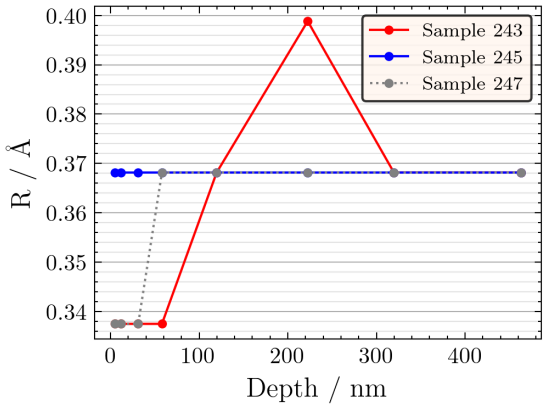

(c) 1. coordination radius (Nb – Nb)

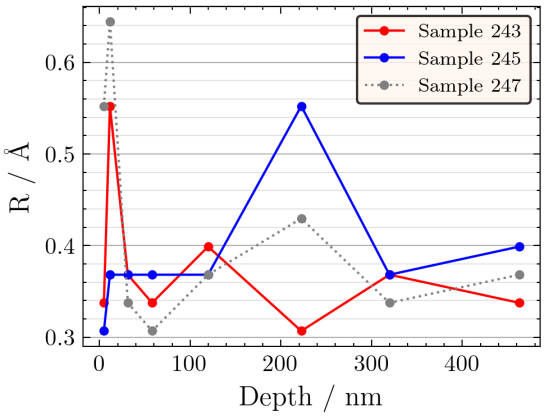

(d) 3. coordination radius (Nb – Nb)

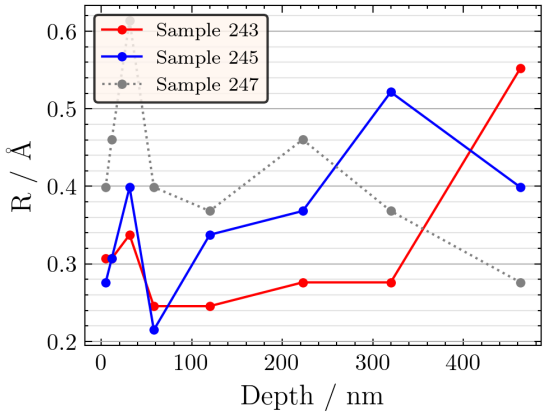

(e) 4. coordination radius (Nb – Nb)

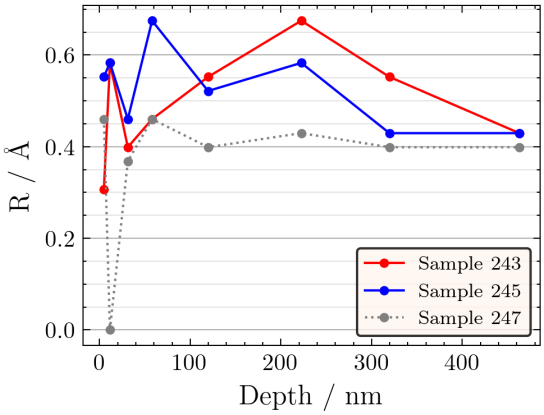

(f) 5. coordination radius (Nb – Nb)

Figure 18: Peak width as a function of the penetration depth.

C Error Plots

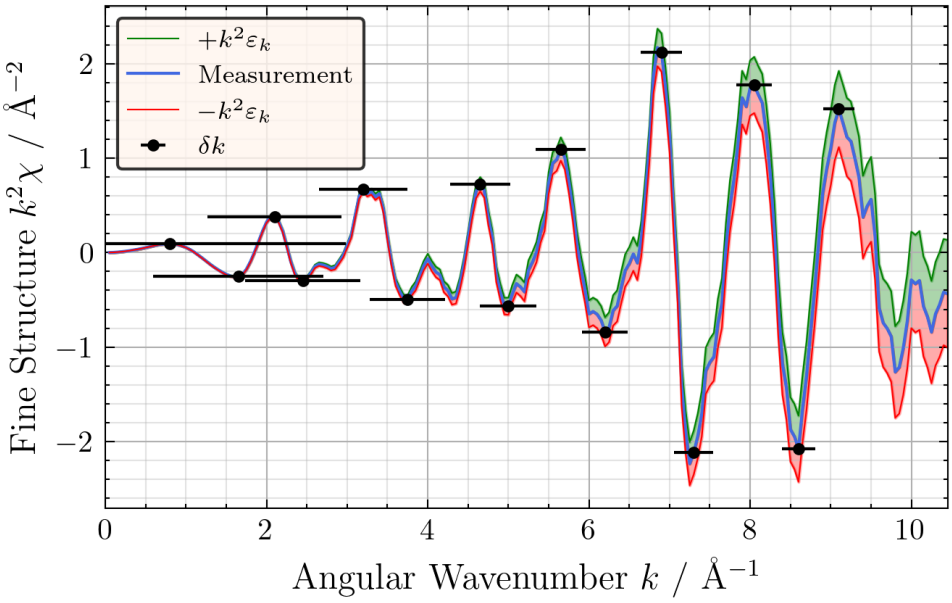

Figure 19: Fluctuation ε_k (k^2-weighted) and resolution δk exemplarily of sample 245 with an angle of incidence $\theta = 0.5°$, according to error analysis in sec. 6.

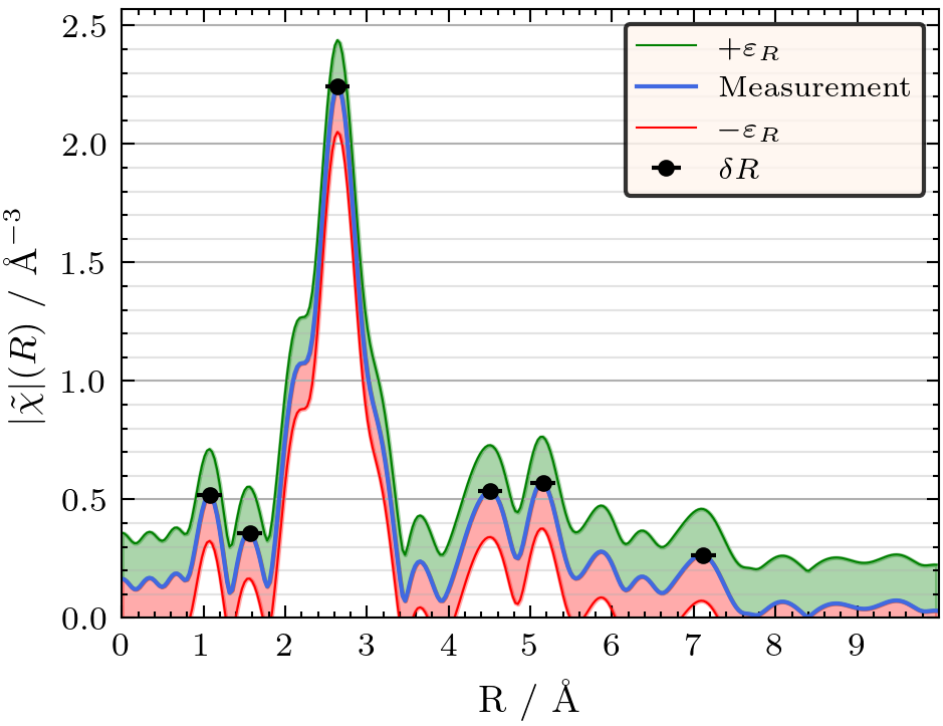

Figure 20: Fluctuation ε_R and resolution δR exemplarily of sample 245 with an angle of incidence $\theta = 0.5°$, according to error analysis in sec. 6.

D Basic Terms of Self-Referencing Systems

Practicing physics, both in the theoretical approach of discussing and inventing models and the experimental approach of discussing and performing analyses, requires an understanding of the research field in order to know which research will be productive and which meaningless[27]. This understanding exists either in the form of knowing what the task is (performing a predefined experiment, calculating a family of integrals for a more general problem, comparing the predictions of several known models following literature, etc.) or knowing how to define an appropriate task (which experiments are promising for a successful analysis of my sample, which models are able to explain a given many-body problem, etc.). Though both forms act together, the latter and only the latter tends to ask the question of 'What should I do to achieve the good?' and is due to the little word 'good', philosophical. Furthermore it's describing a situation where the yet to be given answer (the appropriate task) depends on the situation as a whole (with all it's values, influences and interests) and thus especially on the questioner. In other words, it describes a self-referencial situation.

To return to the point and conclude, practicing physics requires to identificate and deal with self-referencial situations. The more independent a physicist has to work – already increasingly during the process of his/her education –, the more necessary this ability becomes, as best exemplified by the reorientation of research following paradigm shifts, which can occur without warning. In fields where methods, techniques and experience are missing, knowledge about handling self-referencial systems helps moving forward. This does not concern specific fields only, but strictly speaking every single field in science.

For this purpose, terms suitable for analyzing self-referencial systems will be proposed below. The general picture in which we operate is that the physicist is acting as him-/herself, observes natural phenomena inductively, some of which he/she doesn't understand and others trying to describe deductively, in a way that every other physicist could observe them as well, due to that description.

Beginning by defining the term **seref** as representative for self-referencial, the circumstance of knowing what the task is **calcism** and the circumstance of finding the proper task **launism**. The idea is, that these terms represent a more abstract meaning. When a scientist observes reality (nature), he/she is first of all overwhelmed by *launistic* impressions (launism of nature itself), phenomena that he/she does not question but just accepts. This way of experiencing a **seref system** shall be called **serlau** and is supplemented by the term **sercal** for reducing the phenomena of a *seref system* to *calculistic* (e.g. mathematically describable) relations. Because every proposition about a *seref system* (**seref proposition**) can be denied (e.g. the Schrödinger equation of a charged quantum particle in a potential $V(r)$ can be denied as not fundamental by argumenting that a potential cannot be given without taking the solution of the equation of motion into account, which influences the potential $V(r)$ again via the coulomb interaction), it is an intrinsic property of a *seref proposition* that it can be doubted. Such

[27] Hereby, research without a meaningful result isn't necessarily meaningless, because it can help to achieve progress. I take this thesis as a prime example.

doubts should therefore be called **seref doubts**. And the motivation of the physicist to further make propositions although they can be doubted by *seref doubts* is given by the awareness that some proposition will turn out to be *serefically true*[28] for sure. This motivation can thus be called **seref pleasure**.

Now *seref propositions* can be categorized in the case of the proposer in either a proposition motivated through *seref pleasure* due to pure *calculistic* considerations of the proposer (let those be called **sercal pleasure** induced) and motivated through knowingly *launistic* considerations (accordingly called **serlau pleasure** induced). And in case of the doubter of a given *seref proposition*, this can lead to a doubt, that is only some obvious *seref doubt* and thus we obtain a **sercal doubted** *seref proposition* or a doubt, that references to some other *seref proposition* which contradicts the initial one (leading to a **serlau doubted** *seref proposition*).

Reflecting again, *seref systems* do not have a clear rule to determine which proposition about it is true and which is false. Ultimately, however, this can be determined by examining what the case actually was (e.g. the motion of a double pendulum cannot be predicted theoretically due to deterministic chaos, meaning that propositions about it beforehand cannot be called true or false. After observing it's development over time however, such propositions can be verified afterwards). So some *seref propositions* will turn out to be true, even though they could never be proven logically. To describe this dynamic entity of an ongoing (flowing) verification of *seref propositions*, not due to logic but the verdict of reality, it shall be called **flarameter**, which in most cases of physics is given by the continuous parameter of time.

To allow a beneficial use of analyzing *seref systems* for the work of the physicist, it shall rather be discussed by the physicist, which of the propositions he/she made and encountered are induced through **sercal** or **serlau pleasure** and **sercally** or **serlauily doubted**. The **flarameter** will further show, which propositions find confirmation and which not, and thus inspire the researching scientist in his/her more resilient method of critical rationalism. It's discussion will help further research to understand the context back then, to gain imagination for the following.

Finally, a productive research in terms of 'knowing how to define an appropriate task' is accomplished through the following three-part program: First identify those propositions that can be expressed as *seref propositions*. Secondly making sure that all expressed *seref propositions* are induced by *serlau pleasure* and all challenged *seref propositions* (of cited literature) are *serlau doubted*. And lastly providing scenarios of outcomes through the *flarameter* regarding the discussed *seref propositions*.

[28] Meaning that such a proposition is of the property that every other physicist could verify it by him-/herself.

Acknowledgements

This thesis shall be shared with several other people who contributed to it's creation. I want to thank Lennard Luth for introducing me into the field of EXAFS by sharing his knowledge through his own thesis. For performing the beamline experiment, we have learned a lot from the previous attempt which he analyzed. My supervisor Marc Wenskat was regularly available for discussions and helped carry out the experiment in Dortmund. His character trait of developing a deep fascination for his field of research and enthusiastically expressing this to others helped me greatly to find motivation for this work. I can't say that his ideas and visions in general and for this thesis specifically always stand up to the reality of implementation. This lead to repeated failures of considerations, frustration and forced me to make spontaneous changes to our plans. But I think I can say that this has taught me even more about the scientific way of operating and I admire his optimism and willingness to try things out on principle and to link areas that would otherwise probably rarely come together. It matches my ideal understanding of experimental research and I hope he can maintain this ability for himself. Rezvan Ghanbari was very supportive, helped to perform the beamline experiment as well, gave advice for it's success and offered her expertise to gain deeper understanding of the matter. I am very thankful for this, especially since she is very busy with her doctoral thesis. As the representing professor, Wolfgang Hillert expressed critical opinions which I understood as a counterbalance to Marc. I always had his scepticism in mind, which made me confident enough to not content myself with half-hearted answers. Dirk Lützenkirchen-Hecht gave main expertise at the DELTA facility during beamtime and in the theory of EXAFS afterwards, though the communication primarily had to take place virtually between Hamburg and Wuppertal. It was interesting to see a synchrotron experiment performed with all the experience needed in the regular case of unforseen problems. Also I want to thank my friend Ivo Ziesche for TikZ'ing the experimental setup, whose experience with this package is greater than mine and has relieved me of the stress of having to worry about that as well in recent weeks.

Furthermore I'd like to thank Jessica Pfeffer, whose organizational skills helped me transition from my student assistant status to that of a bachelor's student and print this thesis, among other things. Lea Steder familiarized me as supervisor with the general experimental practice of SRF research in the AMTF hall during my student assistant time before. This experience was surely helpful while writing this thesis, to be aware of what the actual purpose of the MSL group is. During the period of water damage in our group's HF lab, I would like to thank everyone who helped with the renovation, especially Carsten Müller, Thorsten Büttner and Detlef Reschke. For me, it was an opportunity to move into a different office that I found more comfortable, but as a student, you benefit greatly from the social space that the HF lab provides. Moreover, I want to thank the student night watch at DELTA during the beam time, who had even longer shifts than I did. Although they locked me in the facility several times, they always unlocked it for me again.

Ultimately, I thank my brother Till, who allowed me to turn the apartment into utter chaos during the demanding last few weeks surrounding our grandmother's illness and the completion of this thesis.

Eidesstattliche Erklärung

Ich versichere, dass ich die Bachelorarbeit selbstständig angefertigt und keine anderen als die angegebenen Hilfsmittel benutzt habe. Alle Stellen, die dem Wortlaut oder dem Sinn nach anderen Werken entnommen sind, habe ich in jedem einzelnen Fall unter genauer Angabe der Quelle deutlich als Entlehnung kenntlich gemacht. Ich versichere, diese Arbeit nicht bereits in gleicher oder ähnlicher Fassung in einem anderen Prüfungsverfahren eingereicht zu haben. Sofern im Zuge der Erstellung der vorliegenden Bachelorarbeit generative Künstliche Intelligenz (gKI) basierte elektronische Hilfsmittel verwendet wurden, versichere ich, dass meine eigene Leistung im Vordergrund stand und dass eine vollständige Dokumentation aller verwendeten Hilfsmittel gemäß der Guten wissenschaftlichen Praxis vorliegt. Ich trage die Verantwortung für eventuell durch die gKI generierte fehlerhafte oder verzerrte Inhalte, fehlerhafte Referenzen, Verstöße gegen das Datenschutz- und Urheberrecht oder Plagiate.

Ich bin damit einverstanden, dass die Bachelorarbeit veröffentlicht wird.

Halstenbek, 19.10.2025,

Ort, Datum, Unterschrift